MID-AMERICA
TRANSPORTATION CENTER

Report # MATC-MST: 345

Final Report
25-1121-0001-345

Initial Study and Verification of a Distributed Fiber Optic Corrosion Monitoring System for Transportation Structures

Hai Xiao, Ph.D.
Associate Professor
Department of Electrical and Computer Engineering
Missouri University of Science and Technology

Genda Chen, Ph.D., P.E., F.ASCE
Professor
Zhan Gao, Ph.D.
Postdoctoral Research Associate
Ying Huang, Ph.D. Candidate
Graduate Research Assistant
Fujian Tang, Ph.D. Candidate
Graduate Research Assistant

2012

A Cooperative Research Project sponsored by the U.S. Department of Transportation Research and Innovative Technology Administration

The contents of this report reflect the views of the authors, who are responsible for the facts and the accuracy of the information presented herein. This document is disseminated under the sponsorship of the Department of Transportation University Transportation Centers Program, in the interest of information exchange. The U.S. Government assumes no liability for the contents or use thereof.

Initial Study and Verification of a Distributed Fiber Optic Corrosion Monitoring System for Transportation Structures

Hai Xiao, Ph.D.
Associate Professor
Department of Electrical & Computer Engineering
Missouri University of Science & Technology

Genda Chen, Ph.D., P.E., F.ASCE
Professor and MATC Associate Director
Department of Civil, Architectural, & Environmental Engineering
Missouri University of Science & Technology

Zhan Gao, Ph.D.
Postdoctoral Research Associate
Department of Electrical & Computer Engineering
Missouri University of Science & Technology

Ying Huang, Ph.D. Candidate
Graduate Research Assistant
Department of Civil, Architectural, & Environmental Engineering
Missouri University of Science & Technology

Fujian Tang, Ph.D. Candidate
Graduate Research Assistant
Department of Electrical & Computer Engineering
Missouri University of Science & Technology

A Report on Research Sponsored by

Mid-America Transportation Center
University of Nebraska–Lincoln
Federal Highway Administration

July 2012

Technical Report Documentation Page

1. Report No. 25-1121-0001-345	2. Government Accession No.	3. Recipient's Catalog No.
4. Title and Subtitle Initial Study and Verification of a Distributed Fiber Optic Corrosion Monitoring System for Transportation Structures		5. Report Date July 2012
		6. Performing Organization Code
7. Author(s) Hai Xiao; Genda Chen; Zhan Gao; Ying Huang; Fujian Tang		8. Performing Organization Report No. 25-1121-0001-345
9. Performing Organization Name and Address Mid-America Transportation Center 2200 Vine St. PO Box 830851 Lincoln, NE 68583-0851		10. Work Unit No. (TRAIS)
		11. Contract or Grant No.
12. Sponsoring Agency Name and Address Research and Innovative Technology Administration 1200 New Jersey Ave., SE Washington, D.C. 20590		13. Type of Report and Period Covered July 2009–March2012
		14. Sponsoring Agency Code MATC TRB RiP No. 24481
15. Supplementary Notes		

16. Abstract

For this study, a novel optical fiber sensing system was developed and tested for the monitoring of corrosion in transportation systems. The optical fiber sensing system consists of a reference long period fiber gratings (LPFG) sensor for corrosive environmental monitoring and a LPFG sensor coated with a thin film of nano iron and silica particles for steel corrosion monitoring. The environmental effects (such as pH and temperature) are compensated by the use of the reference LPFG sensor. The sensor design, simulation, and experimental validation were performed in this study to investigate the feasibility of the proposed sensing system for corrosion and environment monitoring. The detailed investigations of the proposed sensing system showed that within the detection limitation of the thin coated layer, the proposed sensor could monitor both the initial and stable corrosion rate consistently. Compared to the traditional electrochemical method, the proposed optical fiber sensing system has a converter coefficient of 1 nm/day=3.746×10^{-3} A/cm^2. Therefore, the proposed nano iron/silica particles dispersed polyurethane coated optical fiber sensor can monitor the critical corrosion information of the host members in real time and remotely. With multiple LPFGs in a single fiber, it is possible to provide a cost-effective, distributed monitoring solution for corrosion monitoring of large scale transportation structures.

17. Key Words		18. Distribution Statement	
19. Security Classif. (of this report) Unclassified	20. Security Classif. (of this page) Unclassified	21. No. of Pages 48	22. Price

Table of Contents

Acknowledgments ix
Disclaimer x
Abstract xi
Executive Summary xii
Chapter 1 Introduction 1
1.1 Problem Statement 1
1.2 State-of-art/ Literature Review 2
1.3 Objectives in this Research 4
Chapter 2 LPFGs Based Environmental Sensors for Corrosion 6
2.1 Operational Principles of LPFGs 6
2.2 Monitoring of the Environmental Refractive Index Change 7
2.2.1 Operating Principle of using LPFGs for RI Monitoring 7
2.2.2 Experimental Results for Surrounding Refractive Index Detection 8
2.2.3 Sensing of the pH Changes of the Corrosion Environments 9
2.2.4 Sensing of the Chlorate Ion Concentration Changes 10
2.3 Sensing of the Temperature Changes of the Corrosion Environments 11
2.3.1 Operating Principles Temperature Sensing by using LPFGs 11
2.3.2 Experimental Results for Temperature Sensing 12
2.4 Conclusions 13
Chapter 3 LPFGs Based Strain Sensors for Corrosion Monitoring 14
3.1 Operating Principles of LPFG for Strain Sensing 14
3.2 Experiments and Discussion 14
3.3 Conclusions 15
Chapter 4 Mass-sacrificing Corrosion Sensor 17
4.1 Operational Principles & Sensor Design 17
4.1.1 Corrosion Process of Iron Particles 17
4.1.2 Sensor Design 17
4.1.3 Operating Principles of LPFG Based Corrosion Sensor 18
4.2 Coating Procedure & Characterization 19
4.2.1 Coating Composition & Process 19
4.2.2 LPFG Spectrum Change during Sensor Fabrication 20
4.2.3 Coating Characteristics 21
4.3 Compensation for Corrosion Environmental Effects 23
4.3.1 Temperature Compensation 23
4.3.2 pH Change Compensation 24
4.4 Corrosion Monitoring of Nano Iron Particles 25
4.4.1 Test Setup 25
4.4.2 Test Results 26
4.5 Conclusions 28
Chapter 5 Corrosion Monitoring of Steel using Proposed Sensing System 29
5.1 Characterization of the Oxide Layer on the Steel Rebar before Corrosion 29
5.2 Test Setup 30
5.3 Steel Corrosion Monitoring Results and Discussions 32
5.3.1 Oxide Layer Characteristics after Corrosion 32

5.3.2 Steel Corrosion Monitoring Results from Coated LPFG Sensors 34
5.3.3 Discussion of Steel Corrosion Monitoring Results from Coated LPFG Sensors ..37
5.3.4 Characterization of Coated LPFG Sensor after Corrosion Test 38
5.4 Corrosion Measurement Results from Electrochemical Studies 40
5.5 Correlation between the Two Measurement Methods 41
5.5 Conclusions.....41
Chapter 6 Conclusions 43

List of Figures

Figure 2.1 (a) Schematic view of CO_2 laser based LPFG fabrication process and (b) representative LPFG transmission response 7
Figure 2.2 Simulation of the resonant wavelength change of the LPFG (LP_{06}) with various RI ... 8
Figure 2.3 Experimental validation of refractive index detection using LPFGs: (a) Spectrum changes of LP06 in liquids and (b) comparison of resonant wavelength change of the LPFG in various RIs with the simulated results 9
Figure 2.4 Changes in resonant wavelength of an LPFG sensor (LP_{06}) as a function of the pH value 10
Figure 2.5 A bare LPFG in response to NaCl concentration variations in a solution..... 11
Figure 2.6 Changes in resonant wavelength of the LPFG as a function of temperature 12
Figure 3.1 Experimental results of LPFG (LP_{06}) sensor in response to axial strain: (a) Photograph of the test setup, (b) Spectrum change of the LPFG under applied strains, and (c) Resonant wavelength change of the LPFG under various strains..... 15
Figure 4.1 Illustrative structure of an LPFG sensor coated with nano iron particles 18
Figure 4.2 SEM images: (a) Nano iron particles and (b) nano silica particles 19
Figure 4.3 LPFG spectrum change during the coating process 21
Figure 4.4 (a) and (b) Surface and cross sectional SEM images of the polyurethane coating, respectively; (c) and (d) Surface and cross sectional SEM images of the coating with nano iron and silica particles dispersed into polyurethane, respectively; (e) and (f) Surface and cross sectional SEM images the coating with nano iron and silica particles after the heating process..... 23
Figure 4.5 Temperature effects on coated and uncoated LPFGs: (a) Spectrum changes of the coated LPFG, and (b) resonant wavelength changes in response to temperature for the uncoated and coated LPFG sensors. 24
Figure 4.6 pH effect on resonant wavelength: (a) Spectrum changes of the coated LPFG and (b) resonance wavelength changes with pH value for the uncoated and coated sensors..... 25
Figure 4.7 Setup of a proof-of-concept corrosion test 26
Figure 4.8 Proof-of-concept corrosion test results on an LPFG coated with nano iron particles: (a) Large SEM view on the surface condition of a coated fiber after immersion for 30 days, (b) Small SEM view on the surface condition of the coated fiber, (c) cross-section of the coated fiber after corrosion test, and (d) resonant wavelength change of the coated LPFG sensor over time. 28
Figure 5.1 (a) Cross sectional images and (b) the EDS analyses of the steel rebar samples..... 29
Figure 5.2 X-ray diffraction analyses of the oxide layer 30
Figure 5.3 Steel rebars' preparation for corrosion tests..... 31
Figure 5.4 Experimental setup for corrosion monitoring..... 32
Figure 5.5 Comparison of the steel rebar before and after corrosion test for two months 33
Figure 5.6 (a) SEM images of the oxide layer before corrosion test, (b) micro-image of the rust layer after corrosion test, and (c) micro-image of the interface between the steel and the rust..... 34
Figure 5.7 (a) Optical spectrum change of the coated LPFG through the corrosion test, (b) resonant wavelength change versus immersing time, (c) intensity change of the resonant peak versus immersing time, and (d) change rate of the resonant wavelength and its corresponding peak intensity versus immersing time 37

Figure 5.8 Corrosion rate obtained from the monitored results of the coated LPFG through the corrosion test: (a) Corrosion rate in resonant wavelength changes and (b) in intensity changes 38
Figure 5.9 SEM images of the coated LPFG sensor after corrosion tests: (a) surface condition of the coating, (b) cross section of the remaining coating, (c) cross section of the fiber with rust on coating surface, (d) surface of the rust in large scale, (e) surface condition of the rust on the fiber surface in micro-scale, and (f) the small scale of the rust on the fiber surface 39
Figure 5.10 Corrosion rate estimated from potentiodynamic test results 40

List of Tables

Table 5.1 Chemical composition of steel rebar tested 31
Table 5.2 Correlation of steel corrosion from various measurement methods 41

List of Abbreviations

Long period fiber grating (LPFG)
Nondestructive evaluation (NDE)
Fiber Bragg grating (FBG)
Fiber reinforced polymer (FRP)
Single-mode fiber (SMF)
Refractive index (RI)
Scanning electron microscopy (SEM)

Acknowledgements

Financial support to complete this study was provided by Mid-America Transportation Center under Award No. 00026380. Nano silica particles were provided by Dr. Choel-Woon Kim from Mo-Sci Corporation, Rolla, MO. The findings and opinions expressed in the report are those of the authors only and do not necessarily reflect the views of the sponsor.

Disclaimer

The contents of this report reflect the views of the authors, who are responsible for the facts and the accuracy of the information presented herein. This document is disseminated under the sponsorship of the U.S. Department of Transportation's University Transportation Centers Program, in the interest of information exchange. The U.S. Government assumes no liability for the contents or use thereof.

Abstract

For this study, a novel optical fiber sensing system was developed and tested for the monitoring of corrosion in transportation systems. The optical fiber sensing system consists of a reference long period fiber gratings (LPFG) sensor for corrosive environmental monitoring and a LPFG sensor coated with a thin film of nano iron and silica particles for steel corrosion monitoring. The environmental effects (such as pH and temperature) are compensated by the use of the reference LPFG sensor. The sensor design, simulation, and experimental validation were performed in this study to investigate the feasibility of the proposed sensing system for corrosion and environment monitoring. The detailed investigations of the proposed sensing system showed that within the detection limitation of the thin coated layer, the proposed sensor could monitor both the initial and stable corrosion rate consistently. Compared to the traditional electrochemical method, the proposed optical fiber sensing system has a converter coefficient of 1 nm/day=3.746×10^{-3} A/cm^2. Therefore, the proposed nano iron/silica particles dispersed polyurethane coated optical fiber sensor can monitor the critical corrosion information of the host members in real time and remotely. With multiple LPFGs in a single fiber, it is possible to provide a cost-effective, distributed monitoring solution for corrosion monitoring of large scale transportation structures.

Executive Summary

In this study, a novel concept of corrosion sensors was demonstrated feasible for long-term corrosion-induced deterioration assessment of large-scale civil infrastructure, such as bridges. The optical fiber sensing system consists of a reference long period fiber grating (LPFG) sensor for environmental monitoring and a LPFG sensor coated with a thin film of nano iron and silica particles for steel corrosion monitoring.

To monitor steel corrosion, a thin layer of nano iron and silica particles dispersed in polyurethane at room temperature was successfully coated on the surface of a LPFG. The sensor operates by measuring the corrosion-induced refractive index change of the coated thin film. To enhance the optical and mechanical properties of the corrosion sensors, silica particles were added which isolated the iron particles for uniform exposure of them to the corrosive environment. Polyurethane was partially removed from the dried coating when placed in a furnace at 200 °C for one hour to provide a direct access of the iron particles to the corrosive environment. Scanning electron microscopy (SEM) images indicated an average coating thickness was 2.5 μm after heat treatment. High-quality resonant spectrum was observed on the coated LPFG sensor. In comparison with an uncoated grating sensor, the coated LPFG sensor has similar sensitivities to the change in temperature and pH value. Therefore, the coupled temperature and pH effects on corrosion monitoring of the coated sensor can be compensated by deploying a parallel bare LPFG sensor. In comparison with the temperature effect, the pH effect on the sensor is negligible.

The coated corrosion sensor was tested in 3.5wt.% salt solution inside a sealed glass tube for one month. As evidenced from surface and cross sectional SEM images of the coating, some iron particles were oxidized and reduced in size, causing an increase of the resonant wavelength

of the sensor. The thickness of the coating was reduced to approximately 2.26 μm after immersion in the 3.5% NaCl solution for one month, indicating a thickness loss of 0.24 μm or 9.6% thickness reduction compared to the initial coating thickness of 2.5 μm. The resonant wavelength of the coated sensor was found to rapidly increase in the first two weeks but decelerate towards the end of corrosion testing. The total increase of resonant wavelength observed at the completion of testing in one month was approximately 0.45 nm or 9% of the full extent (4.9 nm) in wavelength shift, which is in good agreement with the comparison from the SEM technique.

Accelerated laboratory corrosion tests (3.5% NaCl solution immersing test) were implemented to validate the feasibility of the proposed sensing system. In addition to the optical fiber monitoring system, the electrochemical method was also implemented for comparison and correlations. Within the detection limitation of the thin coated layer, the proposed optical fiber sensors detected two different corrosion rates including a higher corrosion rate of 0.128 nm/hr in the beginning of 20 hours and a relatively lower corrosion rate of 0.019 nm/hr thereafter. Considering that in practical applications the second stage of corrosion rate is usually the one detected by conventional measurement methods, the relatively lower corrosion rate was used as the corrosion rate for comparison and correlations. The proposed optical fiber sensing system has a converter coefficient to the conventional electrochemical method of 1 nm/day=3.746×10^{-3} A/cm^2.

Chapter 1 Introduction

1.1 Problem Statement

When exposed to moist air or oxygenated water, iron/steel is expected to be corroded, forming a red encrustation of iron oxide at the outside of the iron surface, known as rust. Thus, on the surface of an iron-related material, small holes may be pitted by the rust, or the rust may also possibly progress over its area uniformly, which may cause cracks in the involved structural components, resulting in the failure of the components. The progressive development of the rust layer on the surface of the iron, then, becomes a major failure source for an unprotected iron-related structural material.

The occurrence of the iron/steel corrosion requires the simultaneous presence of water and a dissolved acid gas or oxygen, or in some cases just dissolved salts (e.g. brine), which commonly coexist in atmospheric environments. With active corrosive environments, the aging deterioration of civil infrastructures is accelerated by the corrosion of the associated steel structures and reinforcing steel bars in concrete. In countries exposed to ice and snow on the roads, the use of deicing salt makes the situation of iron/steel corrosion even worse. For instance, in the United Kingdom, where the use of salt in the transportation system in winter was estimated to cause 50% of rusting, which induced costs of more 130 million dollars per year for the associated repairs. In the United States, the annual direct cost for the corrosion-related maintenance of US highway bridges was around $8.3 billion, indicated from a recent study by Koch et al. (1), which may be worth nearly 5% of the gross national product. High humidity countries or locations experience the worst corrosive environments: Suriname, Abu Dhabi and Indonesia are at the top on the list of rust-prone climates. For example, in 1990, it was reported that 1,300 kilometers of trans-Alaska pipelines, which were designed to be corrosion-proof for

30 to 40 years, were seriously corroded, resulting in expected repair costs as high as $600 million to $1.5 billion. Therefore, corrosion monitoring and assessment of steel/iron in related steel and reinforced concrete structures is of paramount importance in transportation systems.

1.2 State-of-art/ Literature Review

The current practice for corrosion monitoring and assessment of bridges is mainly based on qualitative visual inspections aided with nondestructive evaluation (NDE) tools. Except for bridge decks, corrosion assessment of bridges is mostly done in small areas at a time. Sensor technologies that can be used to cost-effectively monitor and assess large-scale transportation infrastructures are yet to be developed. The existing sensor technologies for corrosion monitoring can be divided into three approaches: electrochemical, physical, and material sacrificial. In particular, optical fiber sensors have attracted worldwide attentions in recent years due to their unique advantages such as compactness, multi-parameter sensing, distributed sensing, and durability (2).

The electrochemical approach intends to quantify the corrosion-related electrochemical process of steel in a moisture/water environment by measuring either the electrical fields/potentials at the steel surface or the corrosion environmental factors such as chloride content and pH of pore fluids (3, 4). Long period fiber gratings (LPFG) optical sensors have been applied to monitor corrosion environments that can be indirectly related to the corrosion process. Cooper et al. (5) investigated LPFG chemical sensors for real-time in situ detection of corrosion precursors and by-products for the health monitoring and maintenance of aging aircrafts. Three chemical sensors had been developed with optical fiber grating technologies: a moisture sensor, a pH sensor, and a metal ion on sensor. For each LPFG chemical sensor, a unique coating was applied to the surface of the LPFG and optimized for specificity, responsiveness, and reliability.

The electrochemical approach is most commonly used to understand the corrosion mechanism and related remediation methods. However, even if all environmental factors contributing to corrosion are monitored, it can still be a real challenge to draw a definitive conclusion on the rate of corrosion or the mass loss of steel structures since their influence on corrosion can be intertwined and evolve over time.

Physical approach intends to quantify the corrosion-induced degradation of structures by measuring various physical quantities such as strains, ultrasonic and acoustic waves, and magneto-elastic properties (6, 7). Optical fiber Bragg gratings (FBG) sensors were often used to measure corrosion-induced strains and then relate them to their corresponding corrosion condition. One of the first FBG corrosion sensors was proposed by Zheng et al. (8). The corrosion sensor was packaged with fiber reinforced polymers (FRP) and then wrapped around the steel bar to be monitored. More recently, Hua et al. (9) applied Fe-C coated FBG sensors for steel corrosion monitoring. As the coating was corroded away, the Fe-C coating induced a change of strain on the FBG sensor that can be monitored by the FBG resonant wavelength change. The physical approach is suitable for monitoring the structural health condition when the measured strains can be definitively attributed to the effect of corrosion over time. However, often times in practical conditions the strain readings can be misleading due to no-corrosion related factors such as loads and thermal effects.

The material sacrificial approach directly measures the corrosion-induced loss of materials by monitoring, for example, the loss of coated metallic thin film materials (10-12), the change in resistance/conductivity (13), and the change in embedded metal antennas (14). Interferometer-based optical fiber corrosion sensors were developed by coating a thin metal film on the cleaved end or on the side of a fiber., The sensor works by detecting the light intensity

changes as the coated thin film gradually corroded away.. For example, Qiao et al. (10) proposed a thin Fe-C alloy solid film coating and Leung et al. (11) investigated an iron thin film on the cleaved end of an optical fiber for corrosion assessment. Abderrahmane et al. and Benounis (15, 16) proposed optical fiber corrosion sensors with an electroless deposit of Ni-P and aluminum film on the uncladded portion of the fiber. Dong et al. (17) further investigated various metal cladding fibers, including iron (by physical vacuum deposition), nickel (by magnetic field vacuum deposition), and silver (by chemical sputtering/plating). Such a coated optical fiber sensor is simple in concept, but only monitors steel rebar at one point. Multiplexing a large number of interferometer-based sensors becomes a real challenge for the corrosion monitoring of structures in large scale. In addition, metal cladding sensors are vulnerable to installation damage since the optical fiber becomes extremely fragile after an uncladding process. More importantly, the metal cladding likely separates from the optical fiber as corrosion takes place in the metal cladding.

The above brief review indicated that direct monitoring of the corrosion rate or mass loss of steel in a large-scale bridge based on the responses of a fiber grating sensor have not yet been exploited to its full extent with the state-of-the-art development of corrosion sensors.

1.3 Objectives in this Research

The main objective of this study was to demonstrate the feasibility of a self-referencing fiber optic sensor system for in situ monitoring of corrosion. The self-referencing corrosion monitoring system consists of three types of sensors, including a corrosion environment sensor, a strain sensor, and a mass-sacrificing corrosion sensor. These three sensors work collectively for the assessment of the corrosion conditions.

1. A bare LPFG can be used directly for monitoring of the corrosion environment by measuring the chemical concentration related refractive index (RI) change (18). Once the relationships among the pH value, the chlorate ion concentration and the wavelength shift are calibrated, a bare LPFG can be used to monitor the corrosion environment.
2. A bare LPFG can also be used as a strain sensor. When a LPFG was subjected to an increasing strain, its resonance wavelength shifted towards the long wavelength region, indicating the strain sensing capability of the LPFG.
3. The mass-sacrificing corrosion sensor combines the advantages of electrochemical and material sacrificial approaches, and introduces a novel LPFG sensor coated with nano iron particles for the direct monitoring of the corrosion rate of iron particles in a corrosive environment. When deployed in proximity and correlated with a steel bar or member, the optical fiber sensor can provide the corrosion rate of the steel. Long period gratings are first inscribed on a single-mode optical fiber with CO_2 irradiation and then coated with a thin layer of nano iron and silica particles once dispersed into polyurethane. The design, fabrication, calibration, and proof-of-concept test of a prototype corrosion sensor were investigated in detail in this study.

The system, with combined information from multiple sensors, therefore, provides the important information on the corrosion-induced material loss and its corrosion environment (e.g., chloride ion concentration, temperature and strain). Integration and cross-analysis of the three sensors' outputs can generate a comprehensive knowledge of corrosion.

Chapter 2 LPFGs Based Environmental Sensors for Corrosion

2.1 Operational Principles of LPFGs

During the fabrication process of a single mode optic fiber, residual stress is developed between the cladding and core of the fiber. The distribution of the residual stress determines the effective refractive index of the fiber (19). CO_2 laser irradiation can decrease the effective refractive index of the fiber core by releasing the residual stress. As such, CO_2 laser irradiations at predesigned locations can create periodic refractive index modulation in an optical fiber for fabrication of LPFGs.

The schematic view of the CO_2 laser based LPFG fabrication system is presented in figure 2.1(a) (20). A CO_2 laser (SYNRAD, Inc.) is controlled by the computer through the laser controller to produce a desired power. The optical fiber (Corning SMF-28) with its buffer stripped is placed on a three dimensional (3D) motorized translation stage. The focused laser beam is transversely loaded onto the single mode optical fiber. Controlled by a computer, the translation stage moves the fiber at a fixed step for laser exposure, resulting in a periodic refractive index modulation in the fiber core which induces a typical LPFG, as shown in figure 2.1(b). Each valley in figure 2.1(b) corresponds to one cladding mode. The resonant wavelength ($\lambda_{res,m}$) of an LPFG sensor can generally be expressed as a function of its grating period (Λ) and effective refractive indices of the core ($n_{eff,co}$) and the cladding modes LP_{0m} ($n_{eff,cl,m}$) as follows (21, 22):

$$\lambda_{res,m} = (n_{eff,co} - n_{eff,cl,m})\Lambda \tag{2.1}$$

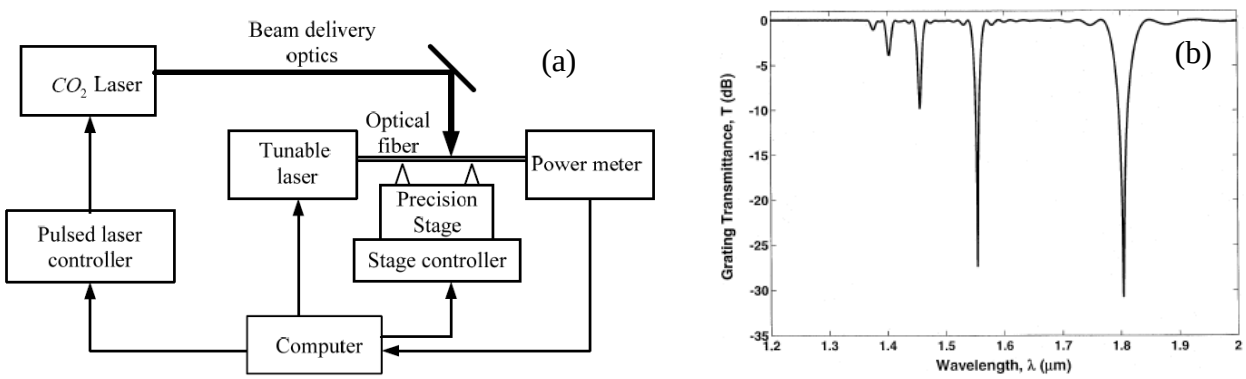

Figure 2.1 (a) Schematic view of CO_2 laser based LPFG fabrication process and (b) representative LPFG transmission response

2.2 Monitoring of the Environmental Refractive Index Change

2.2.1 Operating Principle of using LPFGs for RI Monitoring

When corrosion occurs in aqueous environments, the reference LPFG sensor is able to calibrate/distinguish the refractive index (RI, n_s) changes of the surrounding corrosive liquid when the grating is fully immersed into the corrosion environments. The sensitivity of the LPFG for the surrounding refractive index could be expressed as (22):

$$\frac{\partial \lambda_{res,m}}{\partial n_s} = \lambda_{res,m} \cdot K_{n_s,m} \tag{2.2}$$

where, $K_{n_s,m}$ expresses the dependence of the grating to the surrounding RI for cladding mode m and is defined as (22):

$$K_{n_s,m} = -\gamma_m \cdot \frac{u_m^2 \lambda_{res,m}^3 n_s}{8\pi r_{cl}^3 n_{cl} \left(n_{eff,co} - n_{eff,cl,m}\right)\left(n_{cl}^2 - n_s^2\right)^{\frac{3}{2}}} \tag{2.3}$$

In equation 2.3, γ_m describes the waveguide dispersion for m-th order cladding mode. It is positive for lower cladding modes and negative for higher cladding modes and the turning point of γ_m is dependent on the resonant wavelength range (22).

Simulation of the spectrum change of an LPFG in various surrounding liquids from 1.0 to 1.44 had been performed to the cladding mode of LP_{06} following the procedures provided in Ivanov et al. and Shu (2002) et al. The simulation result of the resonant wavelength change of the LPFG (LP_{06}) as a function of the surrounding RIs is shown in figure 2.2. It is clear that the refractive index change of the surrounding environment can be measured using an LPFG by monitoring its resonant wavelength.

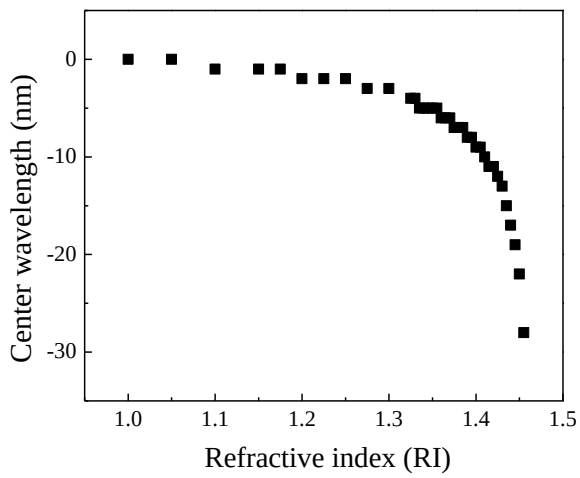

Figure 2.2 Simulation of the resonant wavelength change of the LPFG (LP_{06}) with various RI

2.2.2 Experimental Results for Surrounding Refractive Index Detection

Experiments have been conducted to verify the simulation results and sensor's capability for measurement of surrounding RIs. An LPFG was fabricated using the CO_2 laser system and immersed into liquids of different refractive index. Considering that the commonly used liquids in this study fall into the RI range from 1.33 to 1.44, the investigated surrounding RI of the liquid

is within this range. The liquids used in these experiments included water (n_s=1.33), acetone (n_s=1.36), decane (n_s=1.42), and propylene glycol (n_s=1.432). Figure 2.3(a) shows the spectrum change of an LPFG of the 6th order cladding mode in various surrounding liquids. Figure 2.3(b) shows the comparison of the resonant wavelength shift of the test and that from the simulation results. The experimental results follow the same trade as the simulated curve. The slight difference between the experimental and simulated results may be caused by the variation in concentration of the liquids towards the reference RI values.

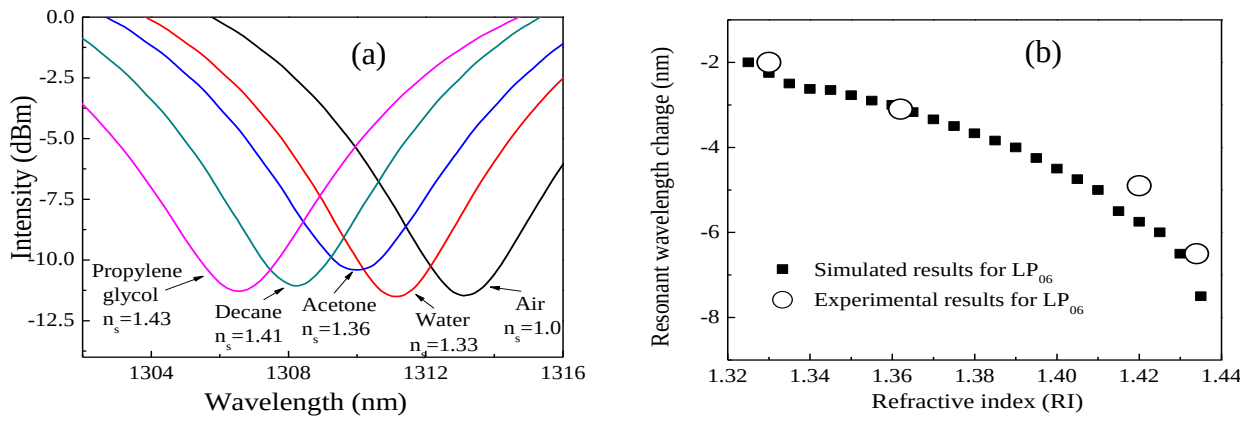

Figure 2.3 Experimental validation of refractive index detection using LPFGs: (a) Spectrum changes of LP06 in liquids and (b) comparison of resonant wavelength change of the LPFG in various RIs with the simulated results

2.2.3 Sensing of the pH Changes of the Corrosion Environments

The pH value has been commonly used in the corrosion environment evaluation. It is known that the refractive index of a liquid depends on the pH value. Therefore, in this study, the relation between the spectrum change (basically resonant wavelength change) of the LPFG sensor and the surrounding pH value change was investigated. An LPFG sensor with a cladding mode of LP_{06} was placed in the solutions with various pH values ranging from 5.8 to 7.8 at 0.4

intervals. Figure 2.4 shows that the resonant wavelength of the LPFG decreases with the pH value approximated linearly as the surrounding pH increases, providing a pH sensitivity of 0.67 nm/pH.

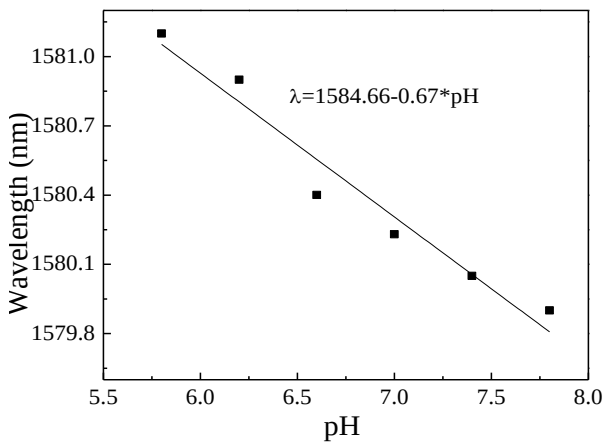

Figure 2.4 Changes in resonant wavelength of an LPFG sensor (LP_{06}) as a function of the pH value

2.2.4 Sensing of the Chlorate Ion Concentration Changes

Another way to study the corrosion environments is to monitor the chlorate ion concentration. The chlorate ion concentration is directly related to the corrosion rate. It is known that a 3.5% weight chlorate ion concentration (commonly found in sea waters) is considered an accelerated corrosion environment. A laboratory test was performed by placing a bare LPFG (LP_{06}) into an NaCl solution with various chlorate ion concentrations. As shown in figure 2.5, the LPFG resonance wavelength shifted towards the short wavelength region as the chlorate ion concentration increased. The relationship between the chlorate ion concentration and the wavelength shift is almost linear.

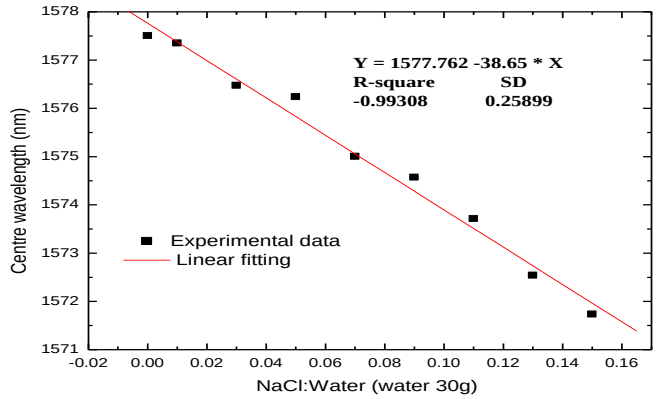

Figure 2.5 A bare LPFG in response to NaCl concentration variations in a solution

2.3 Sensing of the Temperature Changes of the Corrosion Environments

2.3.1 Operating Principles Temperature Sensing by using LPFGs

The induced resonant wavelength shift of the LPFG sensor under a temperature change can be obtained from equation 2.1 and the temperature sensitivity can be expressed as (23-26):

$$\frac{d\lambda_{re,m}}{dT} = \lambda_{D,m}\xi_{T,m} \tag{2.4}$$

in which $\xi_{T,m}$ is the temperature sensitivity coefficient of the LPFG sensor that is determined by (26):

$$\xi_{T,m} = \alpha + \varsigma_{T,m} + \gamma_m \chi_m (2\alpha + \psi_{T,m} + \rho_{co}) \tag{2.5}$$

where:

$$\alpha = \frac{1}{\Lambda}\frac{d\Lambda}{dT}, \tag{2.6}$$

$$\varsigma_{T,m} = \frac{\rho_{co} n_{eff,co} - \rho_{cl,m} n_{eff,cl,m}}{n_{eff,co} - n_{eff,cl,m}}, \tag{2.7}$$

$$\chi_m = \frac{\delta \bar{n}_{eff,co} - \delta \bar{n}_{eff,cl,m}}{n_{eff,co} - n_{eff,cl,m}}, \tag{2.8}$$

$$\psi_{T,m} = \frac{\lambda_{D,m}}{n_{eff,co} - n_{eff,cl,m}} [(\rho_{co} - \varsigma_{T,m}) \frac{dn_{eff,co}}{d\lambda_{D,m}} - (\rho_{cl,m} - \varsigma_{T,m}) \frac{dn_{eff,cl,m}}{d\lambda_{D,m}}]. \quad (2.9)$$

where, α is the thermal expansion coefficient of fiber; $\varsigma_{T,m}$ describes the temperature dependence of the LPFG (25); ρ_{co} and $\rho_{cl,m}$ are the thermo-optic coefficients of core and cladding mode LP_{0m}, respectively; χ_m is the normalized relative effective index change; and $\psi_{T,m}$ represents the wavelength dependence of the temperature sensitivity. For a typical single mode fiber (Corning SMF-28e), $\rho_{co} = 8\times10^{-6} /^o C$ and $\rho_{cl,m} = 7.8\times10^{-6} /^o C$ (23, 24).

2.3.2 Experimental Results for Temperature Sensing

An LPFG sensor was placed in an electric furnace (Thermo Electron Corporation) for verification of the temperature dependence of the grating. It was tested from room temperature to 100 °C at an interval of 20 °C. As shown in figure 2.6, the resonant wavelength of the LPFG increased as a function of temperature. Within the sensing range, the temperature sensitivity of the LPFG sensor is estimated to be 0.04 nm/°C.

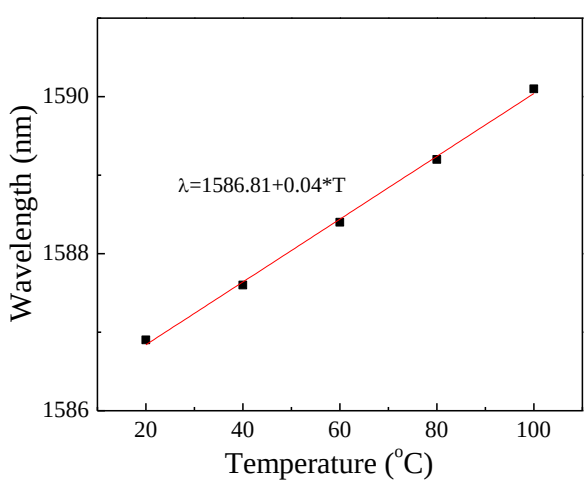

Figure 2.6 Changes in resonant wavelength of the LPFG as a function of temperature

2.4 Conclusions

In this chapter, the sensing capability of a bare LPFG towards the corrosive environmental changes (RI and temperature) was formulated and verified. The operational principles were discussed in detail and laboratory tests for each sensing category were performed. The sensitivities of the LPFG sensor towards the pH value and chlorate ion concentration changes were also calibrated. Test results showed that the LPFG sensors can be used directly for monitoring the corrosion environment by measuring the chemical concentration related refractive index changes and temperature changes.

Chapter 3 LPFGs Based Strain Sensors for Corrosion Monitoring

3.1 Operating Principles of LPFG for Strain Sensing

The resonant wavelength shift of an LPFG sensor induced by an axial strain can be derived from equation 2.1 and expressed into (23-26):

$$\frac{d\lambda_{re,m}}{d\varepsilon} = \lambda_{D,m}\xi_{\varepsilon,m} \tag{3.1}$$

in which $\xi_{\varepsilon,m}$ is the strain sensitivity coefficient of the LPFG sensor. It can be written as (26):

$$\xi_{\varepsilon,m} = 1 + \varsigma_{\varepsilon,m} + \gamma_m \chi_m (2 + \psi_{\varepsilon,m} + \eta_{co}) \tag{3.2}$$

$$\varsigma_{\varepsilon,m} = \frac{\eta_{co} n_{eff,co} - \eta_{cl,m} n_{eff,cl,m}}{n_{eff,co} - n_{eff,cl,m}} \text{ and } \psi_{\varepsilon,m} = \frac{\lambda_{D,m}}{n_{eff,co} - n_{eff,cl,m}} [(\eta_{co} - \varsigma_{\varepsilon,m}) \frac{dn_{eff,co}}{d\lambda_{D,m}} - (\eta_{cl,m} - \varsigma_{\varepsilon,m}) \frac{dn_{eff,cl,m}}{d\lambda_{D,m}}] \tag{3.3}$$

where η_{co} and $\eta_{cl,m}$ are the elastic-optic coefficients of the core and cladding mode LP_{0m} of the LPFG sensor. For a single mode fiber (SMF-28), the elastic-optic coefficients of its core and cladding mode are $\eta_{co} = -0.2219$ and $\eta_{cl,m} = -0.22$ (23, 24), respectively.

3.2 Experiments and Discussion

A series of tension tests were conducted at room temperature. Figure 3.1(a) shows the photograph of the test setup. All tension tests were performed in loading and unloading cycles to verify the repeatability of the sensor. Figure 3.1(b) shows the spectrum change of the LPFG towards strain change. The resonant wavelength of each transmission spectrum was determined and plotted in figure 3.1(c) as a function of the applied strain. It is observed from figure 3.1(c)

that the resonant wavelength of the LPFG sensor changed linearly with the applied strain. The strain sensitivity of the LP_{06} grating was estimated to be 0.00025 nm/με, which was small and may be neglected during corrosion monitoring if other corrosion environmental effects dominate the sensor responses.

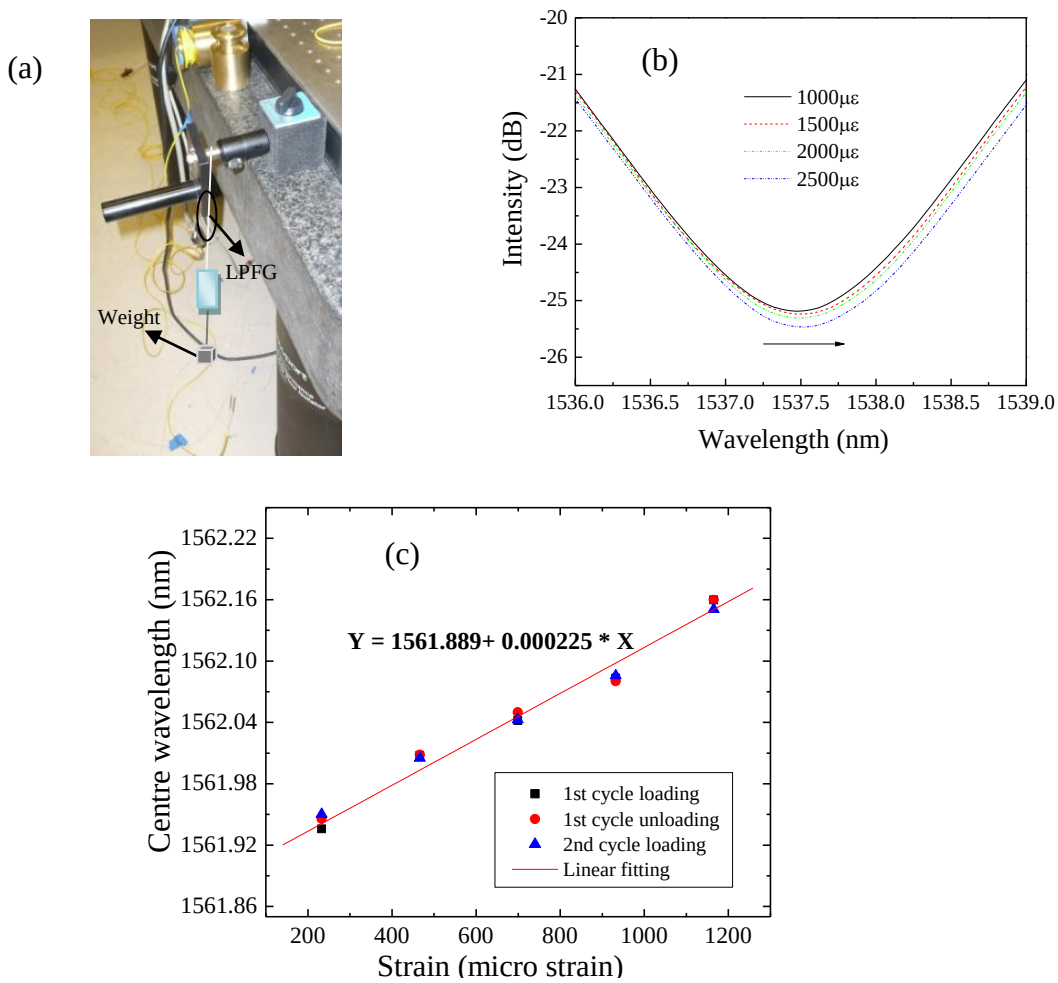

Figure 3.1. Experimental results of LPFG (LP_{06}) sensor in response to axial strain: (a) Photograph of the test setup, (b) Spectrum change of the LPFG under applied strains, and (c) Resonant wavelength change of the LPFG under various strains

3.3 Conclusions

In this chapter, the strain sensitivity of the LPFG sensors was investigated, both theoretically and experimentally. The LP_{06} LPFG has a very small strain sensitivity of 0.00025

nm/με towards the applied axial strain. As a result, the strain effect may be neglected during corrosion monitoring if other corrosion environmental effects dominate.

Chapter 4 Mass-sacrificing Corrosion Sensor

4.1 Operational Principles & Sensor Design

4.1.1 Corrosion Process of Iron Particles

Corrosion of iron particles is an electrochemical process that involves the exchange of electrons. With the presence of moisture and oxygen, the iron particles are oxidized to ferrous ions and prone to migrate toward catholic sites (9, 27) as represented by:

$$2Fe^{2+} + 4OH^{-} \rightarrow 2Fe(OH)_2 \tag{4.1}$$

When sufficient water and oxygen are available, further oxidation of Fe^{2+} to Fe^{3+} occurs as described by:

$$4Fe(OH)_2 + 2H_2O + O_2 \rightarrow 4Fe(OH)_3 \tag{4.2}$$

The hydrated ferric oxide has an orange to red-brown color and is the largest component of rust products of corrosion. In addition, the ferric oxide can be dehydrated into α-Fe_2O_3, which is significantly less dense than that of iron particles. Therefore, the rust products of iron particles often appear to be expanded visually (9, 27).

4.1.2 Sensor design

Figure 4.1 shows a typical structure of the proposed LPFG corrosion sensor with a particles-filled polymer coating. The black and white dots represent the primary nano iron particles and the nano silica particles, respectively. When placed in a corrosive environment, the embedded iron particles are gradually corroded away, resulting in a change of the sensor's

optical properties. The nano silica particles are introduced to improve the transparency of the sensor coating. Together with the polymer, they provide a robust and stable framework of the coating even after all the nano iron particles are corroded completely. Additionally, the polymer coating functions as a buffet/jacket for the LPFG sensor to make it more robust and durable in handling and deployment.

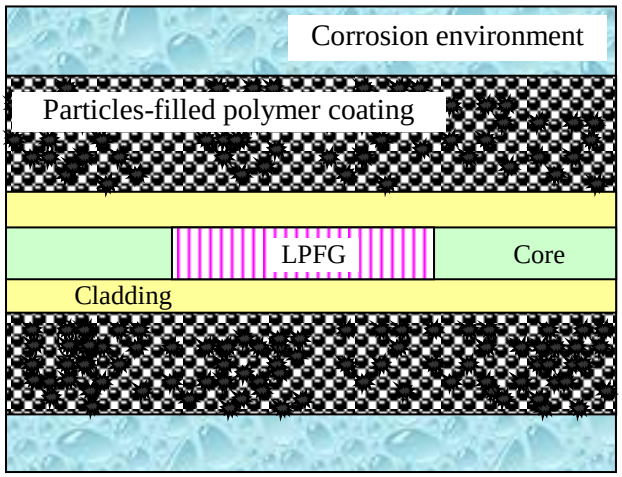

Figure 4.1. Illustrative structure of an LPFG sensor coated with nano iron particles

4.1.3 Operating Principles of LPFG Based Corrosion Sensor

The proposed LPFG based corrosion sensor shown in figure 4.1 operates by monitoring the corrosion induced optical property change of the coated iron-particle thin film. The effective refractive index of the fiber cladding ($n_{eff,cl,m}$) and the thickness of the coated thin film change when the coated iron particles are corroded. As a result, the resonant wavelength of the LPFG changes correspondingly as described by equation 2.1. Therefore, monitoring of the change in the resonant wavelength of the LPFG sensor provides key information about the mass loss and the material property change of the iron particles over time in a corrosive environment. When

deployed in proximity to a steel member or a reinforcing bar, the calibrated sensor provides the corrosion condition of the steel with a pre-determined steel-particle corrosion correlation curve.

4.2 Coating Procedure & Characterization

4.2.1 Coating Composition & Process

Among the many coating materials (polyurethane, polydimethylsiloxane, agarose gel, and ceramic bond) tested in this study, polyurethane was identified as the best candidate which facilitates the adhesion of nano iron and silica particles to the surface of an LPFG sensor due to its uniformity and bonding strength with the optical fiber. The polyurethane used in the coating was prepared by mixing isocyanate with polyol in a 1:1 ratio by weight. The nano iron particles used in this study have a maximum diameter of 100 nm, as shown in the scanning electron microscopy (SEM) image (fig. 4.2(a)). The chemical compositions of the nano iron particles include: Fe 99%, Al 0.018%, Ti 0.0013%, Mo 0.0035%, Ca 0.0035%, Ni 0.002%, Pb 0.001%, Sn 0.002%, Cr 0.0038%, Cu 0.03%, Mg 0.001%, Mn 0.0075%, and Si 0.0025%. The nano silica particles (glass beads) have an average diameter of 7 nm, as shown in figure 4.2(b).

(a)

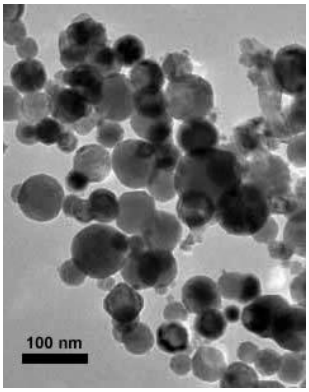

(b)

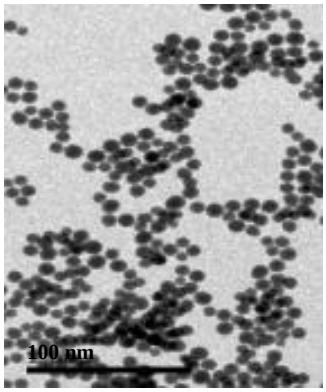

Figure 4.2 SEM images: (a) Nano iron particles and (b) nano silica particles

Nano particles were coated on the optical fiber surface with a dip coating process after they had been dispersed into the polyurethane-acetone solution. First, polyurethane was diluted into acetone by a weight ratio of 1:20 (polyurethane: acetone). The nano iron and silica particles were then added into the polyurethane-acetone solution by a weight ratio of 1:2:80:1600 (silica particles: iron particles: polyurethane: acetone). Next, the solution was placed into an ultrasonic vibrator for 30 minutes of stirring to uniformly disperse nano particles into polyurethane. It was followed by holding the optical fiber with LPFG gratings in a horizontal position and submerging it into the stirred solution for 30 minutes, and horizontally lifting up the coated sensor to air dry for one hour. Finally, the coated fiber was heated at 200 °C for one hour in order to remove part of the polyurethane and give pathways for direct access of moisture to the iron particles. Note that it is important to maintain the horizontal position of the optical fiber during the entire wetting process to minimize potential gravity effects.

4.2.2 LPFG Spectrum Change during Sensor Fabrication

The LPFG sensors used in this study were induced by the CO_2 laser irradiation method and fabricated by closely following the previous study (20). The addition of a thin coated film on the LPFG surface not only changed the fiber surface condition, but also altered the fiber optical property. Figure 4.3 shows how the LPFG spectrum changed during the coating process. The monitored cladding mode of the LPFG is LP_{06} with an initial resonant wavelength of 1586.9 nm and a peak resonant intensity of -30 dB. Throughout the dip coating process, both the resonant wavelength and intensity of the LPFG changed. The resonant wavelength first reduced to 1576.2 nm in the polyurethane-acetone solution, then increased to 1578.8 nm when dried, and further increased to 1582 nm at the completion of coating. The net change in resonant wavelength was 4.9 nm from 1586.9 nm (bare fiber) to 1582 nm (coated fiber) with a corresponding drop of

approximately -5 dB in intensity of the grating. This drop corresponds to approximately 17% of the initial resonant peak. The small changes both in resonant wavelength and intensity of the LPFG, after the coating process was completed, indicated that the film coated on the fiber surface was very thin.

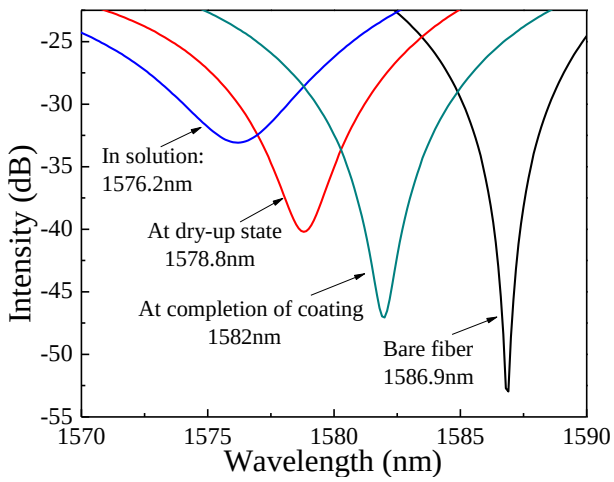

Figure 4.3 LPFG spectrum change during the coating process

4.2.3 Coating Characteristics

The microstructure of the coated LPFG sensor was examined throughout the coating process. Figures 4.4(a) and (b) show the SEM images of the surface condition and cross section of the fiber when coated with the polyurethane-acetone solution only. The polyurethane coating on the fiber surface was uniform and approximately 3.5 μm in thickness. Figures 4.4(c) and (d) show the SEM images of the surface condition and cross section of the optimal fiber when coated with the polyurethane-acetone-nano iron/silica particle solution. The coating became more uniform with a smooth surface but remained approximately 3.5 μm thick after the nano iron and silica particles were dispersed into polyurethane. Figures 4.4(e) and (f) show the SEM images of the surface condition and cross section of the optical fiber after the heating process.

Clearly, the heating process removed part of the polyurethane and the surface condition of the coating became porous, which provided a direct moisture access from the surrounding environment to the iron particles. The thickness of the coating after the heating process was reduced to about 2.5 μm and the coating was uniformly distributed along the fiber cross-section.

(a)

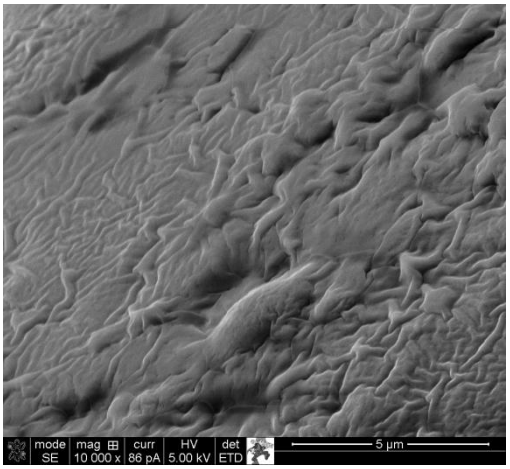

(b)

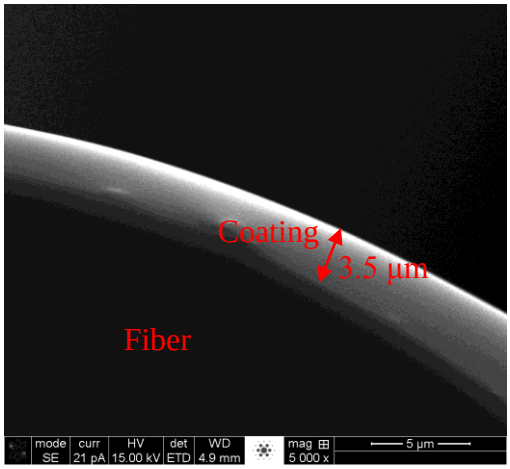

(c)

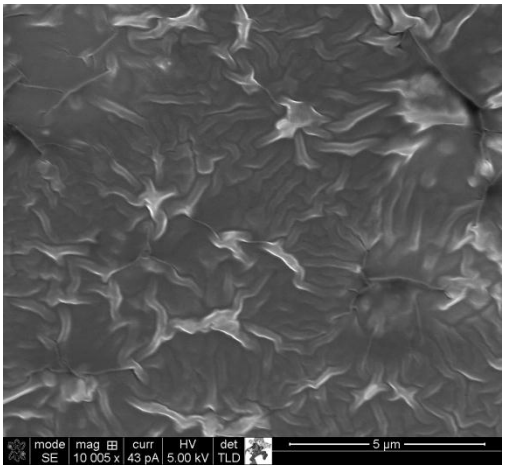

(d)

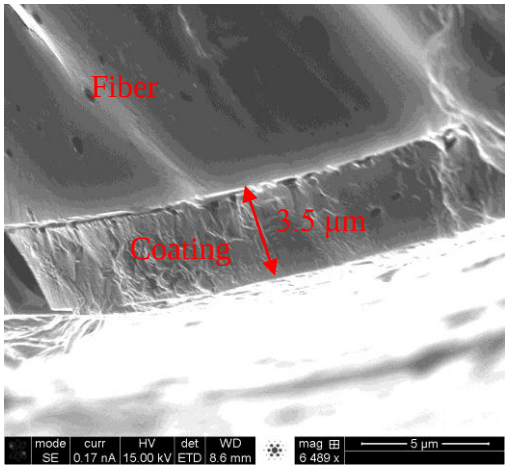

(e) (f)

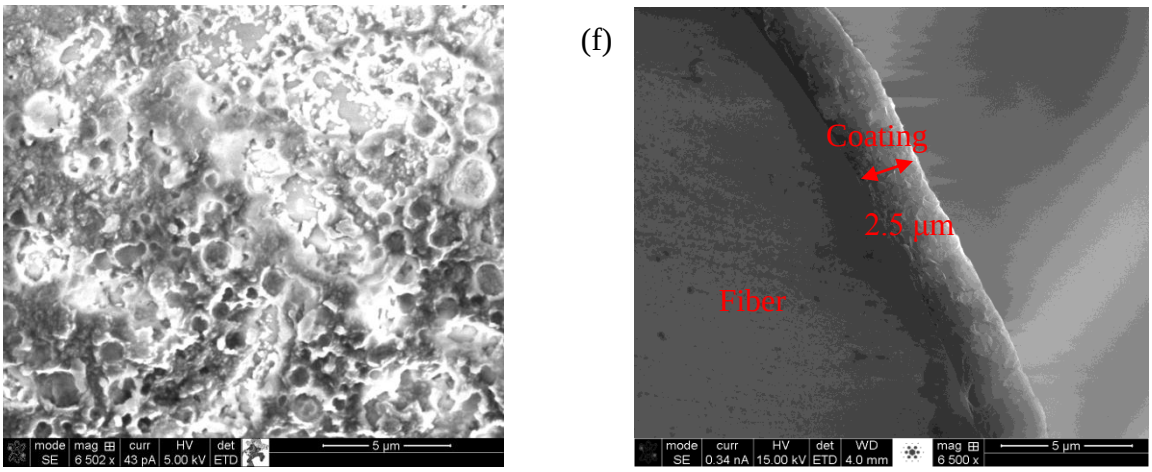

Figure 4.4 (a) and (b) Surface and cross sectional SEM images of the polyurethane coating, respectively; (c) and (d) Surface and cross sectional SEM images of the coating with nano iron and silica particles dispersed into polyurethane, respectively; (e) and (f) Surface and cross sectional SEM images the coating with nano iron and silica particles after the heating process, respectively

4.3 Compensation for Corrosion Environment Effects

In addition to the signals induced by the corrosion of nano iron particles, the corrosion environment changes may also influence the sensor. The two key environmental factors that have been considered in most corrosion studies are temperature and pH change since they are directly related to steel corrosion in the presence of water and oxygen. The LPFG sensors coated with nano iron and silica particles are not only sensitive to the corrosion induced changes in the iron particle embedded thin films, but also to environmental factors such as temperature and pH change. To compensate for the effects of temperature and pH value, a series of tests were conducted to investigate the sensing properties of the LFPG sensor coated with iron particles in various environmental conditions.

4.3.1 Temperature Compensation

An uncoated LPFG sensor and a coated LPFG sensor with iron particles were placed side-by-side in a furnace for temperature measurement and correlation. They were tested under

room temperature to 100 °C at the interval of 20 °C. Figure 4.5(a) presents the spectra of the coated LPFG sensor (LP_{06}) under various temperatures, and figure 4.5(b) plots the resonant wavelength increase as a function of temperature for both the uncoated and coated sensors. Within a sensing range of 100 °C, the temperature sensitivity of the coated LPFG sensor slightly increases from 0.04 nm/°C to 0.455 nm/°C. Therefore, for a temperature change of less than 50 °C, the difference in resonant wavelength is less than 0.275 nm, which is approximately 4% of the total shift in resonant wavelength at room temperature from the uncoated to coated sensor. As such, by deploying an uncoated reference LPFG sensor near the coated LPFG sensor, the temperature effect can be monitored and compensated in corrosion monitoring.

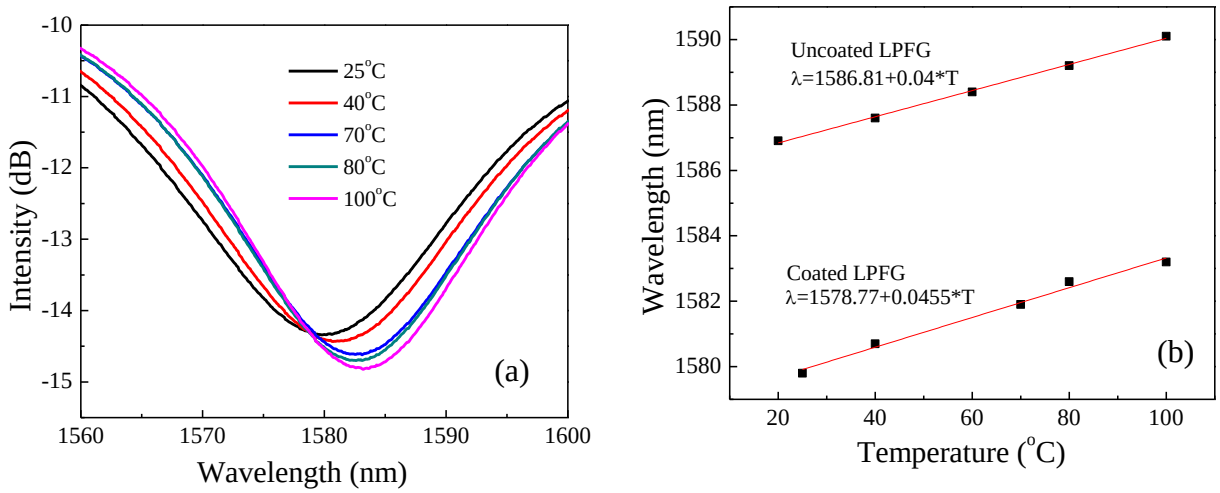

Figure 4.5 Temperature effects on coated and uncoated LPFGs: (a) Spectrum changes of the coated LPFG, and (b) resonant wavelength changes in response to temperature for the uncoated and coated LPFG sensors

4.3.2 pH Change Compensation

The uncoated and coated LPFG sensors were then placed in solutions with various pH values ranging from 5.8 to 7.8 at 0.4 intervals. Figure 4.6(a) presents the spectrum changes of the

coated LPFG (LP_{06}) as the pH value changes, and figure 4.6(b) compares the resonant wavelength change as a function of the pH value between the uncoated and coated sensors. The pH sensitivity of the LPFG sensor slightly decreased from 0.67 nm/°C for the uncoated sensor to 0.66 nm/°C for the coated sensor. For a pH range of less than 2, the difference in resonant wavelength is only 0.02 nm, which is 0.25% of the shift in resonant wavelength from the uncoated to coated sensor at pH = 7. In comparison with the temperature effect, the pH influence to corrosion monitoring is negligible.

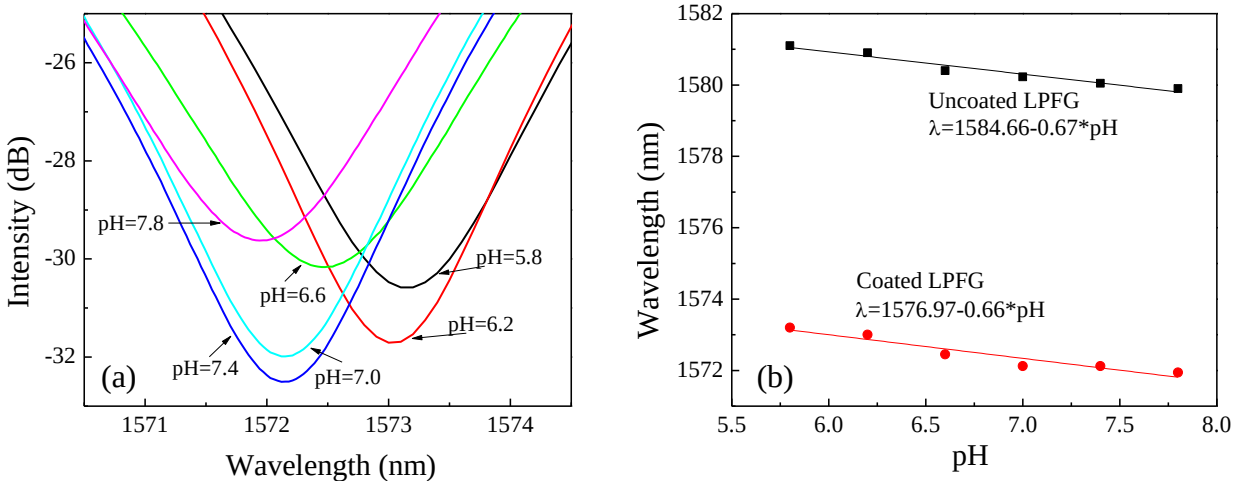

Figure 4.6 pH effect on resonant wavelength: (a) Spectrum changes of the coated LPFG and (b) resonance wavelength changes with pH value for the uncoated and coated sensors

4.4 Corrosion Monitoring of Nano Iron Particles

4.4.1 Test Setup

A proof-of-concept test was conducted at room temperature for the corrosion monitoring of nano iron particles with the proposed LPFG sensor. An accelerated corrosion test was set up as shown in figure 4.7, consisting of a glass tube holding corrosive liquids, an optical spectrum analyzer (OSA, HP70952B), and a personal computer. A nano iron particle coated LPFG sensor

and a reference uncoated LPFG sensor were placed in the transparent tube with one end sealed tightly. After having been filled with 3.5 wt.% NaCl solution, the glass tube was tightly sealed at the other end. The coated and uncoated LPFG sensors were connected in series to a broadband light source ranging from 1520 nm to 1620 nm and the OSA. The light source (LS) was a multiplexed C-band (BBS 1550A-TS) and L-band (HWT-BS-L-P-FC/UPC-B) Erbium Doped fiber amplified spontaneous emission sources. The personal computer (PC) was connected to the OSA for data recording and processing.

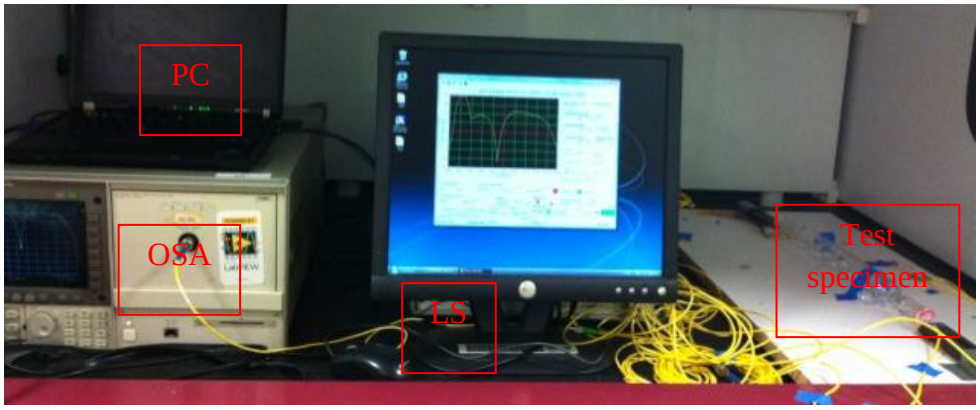

Figure 4.7 Setup of a proof-of-concept corrosion test

4.4.2 Test Results

Figures 4.8(a) and (b) show the SEM images of the coated LPFG sensor in large (5 μm) and small scales (2 μm), and figure 4.8(c) shows the cross-section of the coating after having been immersed in the NaCl solution for one month. During the corrosion test, a significant number of nano iron particles were corroded near the outer surface of the sensor coating, leaving behind localized cavities, as seen in figures 4.8(a) and (b) when compared with the uncorroded sensor shown in figure 4.4(e). The localized cavities, as a result of the iron particles corroded

away, decreased the effective thickness of the thin film, resulting in a resonant wavelength increase of the LPFG sensor over time, as shown in figure 4.8(d). Figure 4.8(c) shows that the thickness of the coating was reduced to approximately 2.26 μm after the coating had been immersed in the 3.5% NaCl solution for one month, indicating a thickness loss of 0.24 μm or a 9.6% thickness reduction compared to the 2.5 μm initial coating thickness. Figure 4.8(d) also shows that a shift of approximately 0.4 nm in resonant wavelength (LP_{06}) rapidly occurred in the first two weeks. After that, the resonant wavelength gradually increased since the coated fiber was placed inside the sealed glass tube and corrosion slowed down as oxygen was reduced over the time. The increase in resonant wavelength at the end of corrosion testing, approximately 0.45 nm, corresponds to approximately 9% of the total wavelength shift (4.9 nm from fig. 2.3) before and after coating. The effective thickness reduction predicted from the spectrum monitoring of the LPFG agrees well with that obtained from the SEM images. In applications, the full extent of the resonant wavelength shift (4.9 nm) can be used to assess the corrosion condition of steel members over a long period of time when installed adjacent to each steel member.

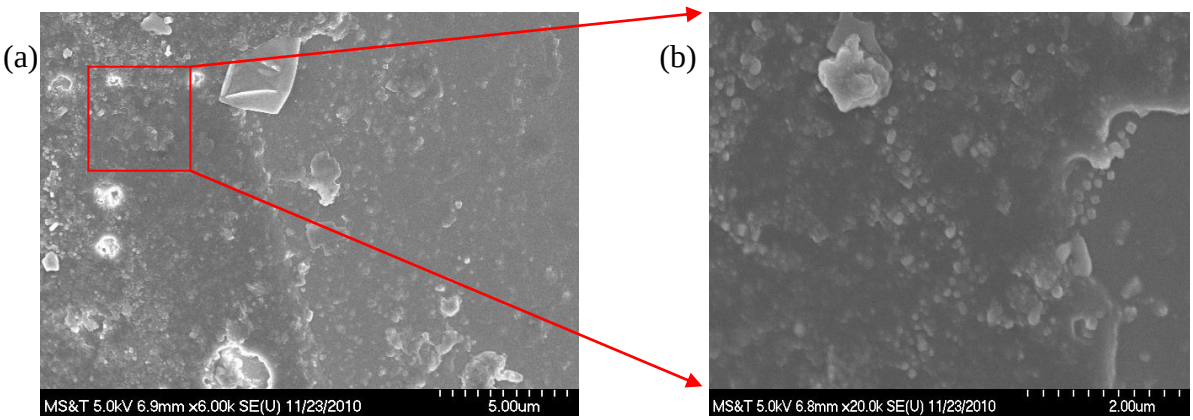

(c)

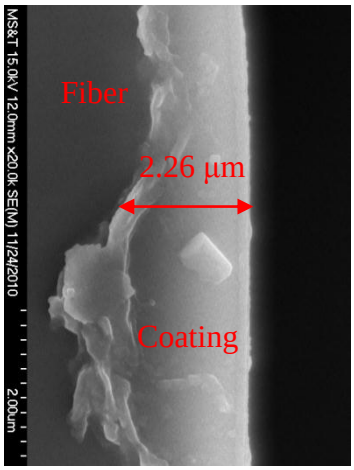

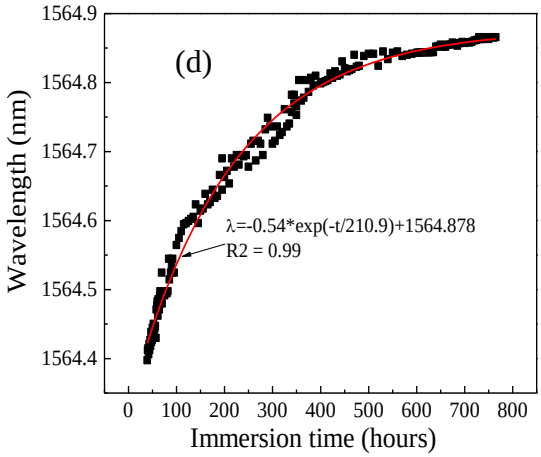

Figure 4.8 Proof-of-concept corrosion test results on an LPFG coated with nano iron particles: (a) Large SEM view on the surface condition of a coated fiber after immersion for 30 days, (b) Small SEM view on the surface condition of the coated fiber, (c) cross-section of the coated fiber after corrosion test, and (d) resonant wavelength change of the coated LPFG sensor over time

4.5 Conclusions

In this chapter, the concept of the proposed fiber optic corrosion sensor was demonstrated feasible for potential applications in a long-term corrosion-induced deterioration assessment of large-scale civil infrastructure, such as bridges. The corrosion sensor was made by coating a long period fiber grating with a thin layer of polyurethane, dispersed with nano iron and silica particles. As the iron particles were gradually corroded away, the resonant wavelength of the optical sensor increased. After calibration, when installed near steel members and correlated with the corrosion process, a group of grating sensors was multiplexed to monitor corrosion induced mass loss of the steel members in a bridge system or a bridge network.

Chapter 5 Corrosion Monitoring of Steel using Proposed Sensing System

5.1 Characterization of the Oxide Layer on the Steel Rebar before Corrosion

The phase composition of the oxide layer of the steel rebar before corrosion tests were examined with X-ray diffraction (XRD, Philip X' Pert). The microstructure and the elemental distribution were investigated using scanning electron microscopy and an energy dispersive spectrometer (EDS) as well. For SEM measurements, a sample with 4.0 mm cross-sectional thickness was cut from the steel rebar, and then consecutively polished with silicate carbide papers with grits of 80, 180, 320, 600, 800 and 1200. Mounting epoxy was cast around the samples to protect the coating from damage during the sample preparation.

Figure 5.1 shows the cross sectional images and the EDS analyses of the steel rebar samples. The steel rebar has a thin (about 25μm thick) oxide layer on the rebar surface, mainly consisting of iron (Fe) and oxygen (O).

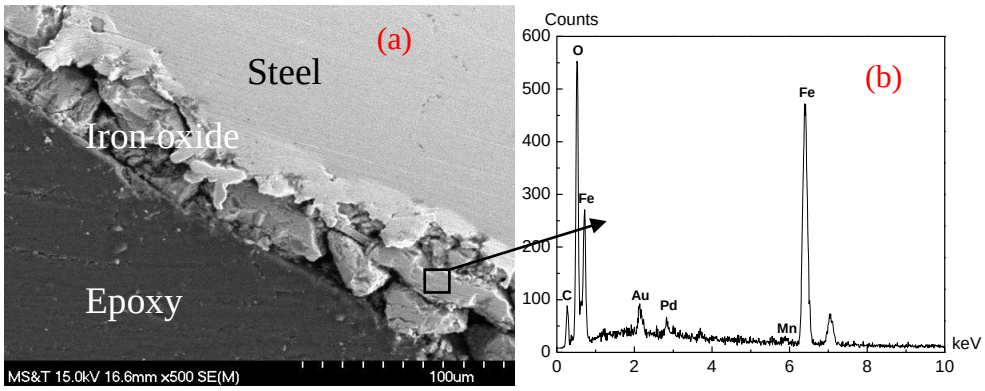

Figure 5.1 (a) Cross sectional images and (b) the EDS analyses of the steel rebar samples

Figure 5.2 shows the X-ray diffraction analyses of the oxide layer formed on the surface of the uncoated rebar prior to corrosion testing. Magnetite (Fe_3O_4) and Maghemite (Fe_2O_3) are the two main oxides on the steel rebar surface.

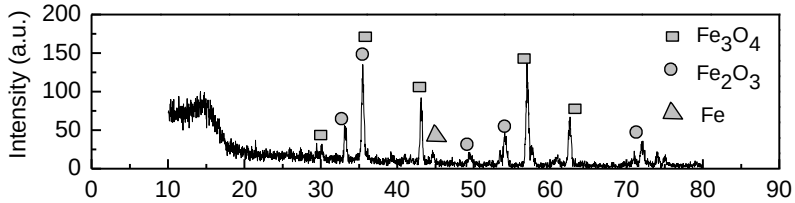

Figure 5.2 X-ray diffraction analyses of the oxide layer

5.2 Test Setup

Steel rebar was selected as the investigating subject in this study, with the consideration of its wide application in concrete reinforced structures. Figure 5.3 shows the preparation of the test steel bars and table 5.1 provides the chemical composition of test steel rebar. With 0.383% carbon contained in the steel rebar, the test specimen was categorized as mild carbon steel. To get a uniform corrosion in the middle of the rebar, epoxy was applied to both ends of the steel rebar by placing the epoxy into a small section of PVC tubes. Channels on the surface of the steel bars were prepared for the installation purpose of the coated LPFG corrosion sensors and the associated environmental referencing LPFG sensors. At one end of the steel rebar, electrical wires were installed to monitor the corrosion rate through traditional electro-chemical methods, in which a potentiodynamic test was implemented for the test steel rebar for a corrosion rate estimation.

Figure 5.3 Steel rebars' preparation for corrosion tests

Table 5.1 Chemical composition of steel rebar tested

Element	C	Si	Mn	P	S	Cr	Mo	Ni	Cu	V	Sn	Fe
Wt. %	0.383	0.184	1.000	0.115	0.064	0.103	0.069	0.198	0.373	0.022	0.028	97.40

To verify the feasibility of the proposed nano iron/silica particle dispersed polyurethane coated LPFG sensor for corrosion monitoring, an accelerated corrosion test was performed in the laboratory, as shown in figure 5.4. Three specimens of steel rebar were immersed into a sodium chloride solution with a weight ratio of 3.5%. The test was conducted in a chamber with a controlled temperature at 25°C. On each rebar, a nano iron/silica particle dispersed polyurethane coated LPFG sensor (for corrosion monitoring) and a reference uncoated LPFG sensor (for corrosion environmental monitoring) were attached to the surface of the steel rebar. Considering that the strain sensitivity of the LPFG sensors are relatively small compared to the environmental changes, the strain effect was neglected in the validation tests. The corrosion related thickness change of the coating, then, was compensated by the corrosion environmental changes.

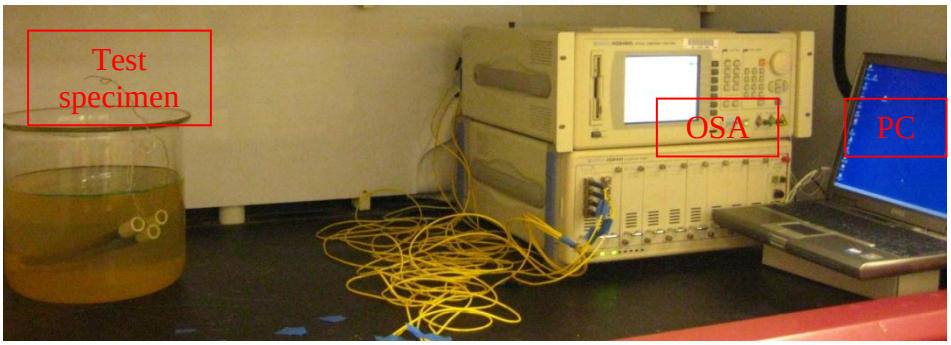

Figure 5.4 Experimental setup for corrosion monitoring

As shown in figure 5.4, all the coated and uncoated LPFG sensors were connected to a broadband light source and an optical spectrum analyzer (OSA, HP 70952B). The broadband light source ranging from 1520 nm to 1620 nm was generated by multiplexing a C-band (BBS 1550A-TS) and an L-band (HWT-BS-L-P-FC/UPC-B) Erbium Doped fiber amplified spontaneous emission. A personal computer was connected to the OSA for data recording and processing. To realize real-time monitoring, the data from the optical fiber sensors were recorded and processed every minute. In addition to the proposed optical fiber sensors, for comparison, electronic wires were embedded on the steel rebar for electrochemical measurements. A potentiodynamic test was implemented for the test steel rebar for a corrosion rate estimation.

5.3 Steel Corrosion Monitoring Results and Discussions

5.3.1 Oxide Layer Characteristics after Corrosion

Figure 5.5 shows the steel rebar before and after two months of an accelerated corrosion test, where a thick layer of oxide (rust) was formed outside of the steel rebar.

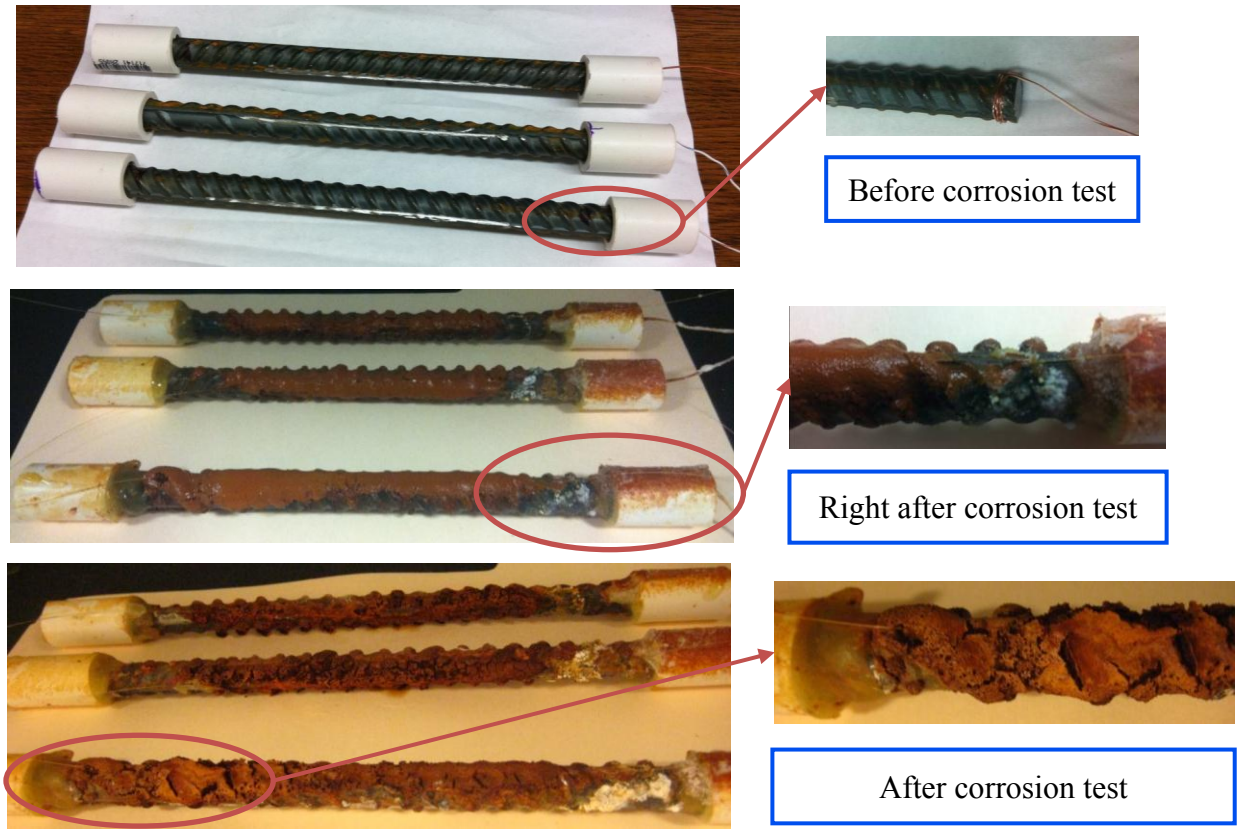

Figure 5.5 Comparison of the steel rebar before and after corrosion test for two months

The thickness of the oxide (rust) layer was evaluated using microscopic tools. The whole scale comparison of the thickness of the rust layer (oxide layer) before and after the corrosion test from the microscope is presented in figures 5.6(a) through (c). Before the corrosion test, the oxide layer on the steel rebar was about 25μm, and after one month of corrosion, the rust layer on top of the steel grew up to more than 2mm in depth, indicating an occurrence of a large extent of corrosion.

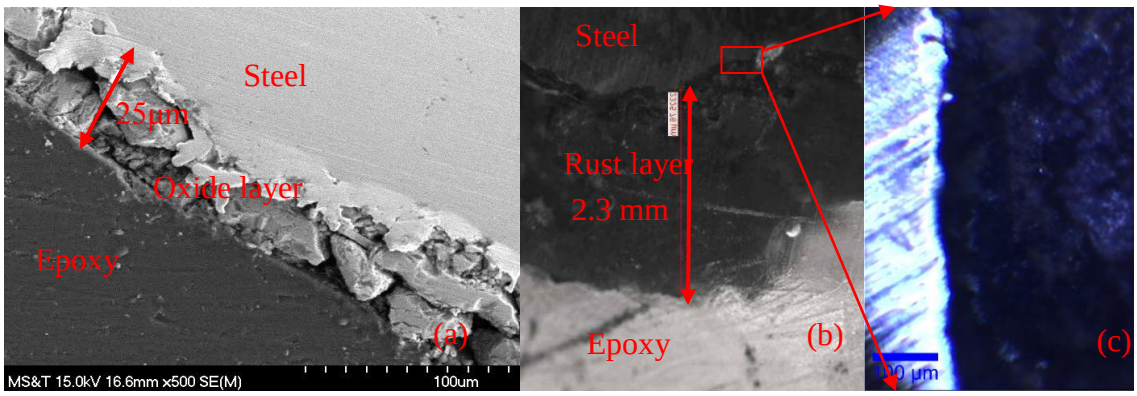

Figure 5.6 (a) SEM images of the oxide layer before corrosion test, (b) micro-image of the rust layer after corrosion test, and (c) micro-image of the interface between the steel and the rust

5.3.2 Steel Corrosion Monitoring Results from Coated LPFG Sensors

Figure 5.7(a) plots the optical spectrum change of the LPFG corrosion sensor in every hour throughout the corrosion test. As the immersing time increased, not only did the resonant wavelength of the coated LPFGs shift right continuously, but also the intensity of the resonant peak dropped significantly. Figure 5.7(b) shows the corresponding resonant wavelength change of the resonant as immersing time increased after taking out the reference. The resonant wavelength of the coated LPFG changed dramatically during the first two weeks (336 hours) from 1573.3 nm to around 1580 nm. The resonant wavelength of the coated LPFG remained around 1580 nm afterwards. Two main reasons may account for the saturation. The first reason could be the limited initial coating thickness of 2.5μm. Once the corrosion penetrated the entire coating layer, no more corrosion induced optical property changes could be detected. In the experiments, after 200 hours of real-time monitoring, the resonant wavelength of the coated LPFG reached 1580 nm, approaching its detection limit of 1580.2 nm. In this case, the coated LPFG has its limited service life restricted by the initial coating thickness and in practical

applications the initial coating thickness needs to be designed based on specific requirements and the designated service life of the components.

The second reason for the stabilized signal could be intrinsic to the corrosion process. After the formation of the outside oxide layer on the steel surface after initial corrosion, further corrosion was slowed down and thus decreased the corrosion rate. Therefore, after one month of corrosion, the corrosion process became stable and yielded a small change of the coated LPFG spectrum.

Figure 5.7(c) shows the resonant intensity change of the coated LPFG sensor versus the immersing time. The intensity of the resonant peak of the LPFG sensors may be influenced by the coating thickness and the thickness of the rust layer of the steel rebar. The intensity of the resonant peak dropped significantly as the corrosion progressed, indicating that the rust layer of the steel covered on the coated LPFG sensor. On the first day (24 hours), the intensity of the resonant changed dramatically from -40.4 dB to -21.4 dB, indicating that the rust layer on the steel rebar formed within one day after the rebar had been placed into the 3.5% sodium chloride solution. After that, the intensity of the resonant peak increased slowly as the immersing time increased, indicating that the resonant peak intensity became insensitive to further increasing as the rust thickness increased to a certain amount.

Figure 5.7(d) shows the change rate of the resonant wavelength and intensity of the coated LPFG after compensation of the environmental effects. Within 30 hours after the specimen was placed into the corrosive solution, the change rate of the resonant wavelength and that of the resonant intensity showed a turning point, where the rate of change turned from increasing to decreasing. The turning point of the resonant intensity change rate was showed at 6.8 hours after the starting of the test, with a rate of 1.53dB/hr. The behavior of the maximum

resonant intensity change rate indicated that the rust layer on the steel surface had uniformly formed along the steel rebar and covered the surface of the coated fiber. From this point on, the change rate of the resonant intensity decreased gradually as the immersing time increased. After 500 hours of corrosion testing, the change rate of the resonant intensity still had a value of 0.041dB/hr. The turning point of the resonant wavelength change rate was located at 20 hours after the starting of the test at a change rate of 0.186 nm/hr, indicating that before the formation of the relatively thick rust layer outside the steel rebar, the corrosion rate of the steel increased significantly. After 20 hours from the starting of the test when the rust layer uniformly generated outside the steel rebar, the corrosion was partially obstructed by the rust layer and slowed down. The resonant wavelength change rate of the coated LPFG rational decreased from 0.186 nm/hr at the turning point to 0.0125 nm/hr at one month after.

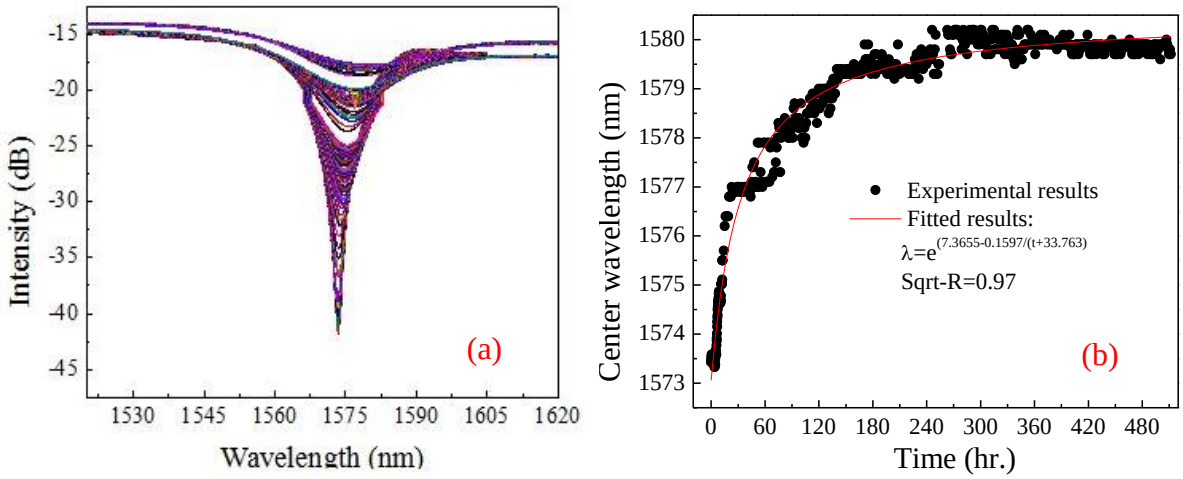

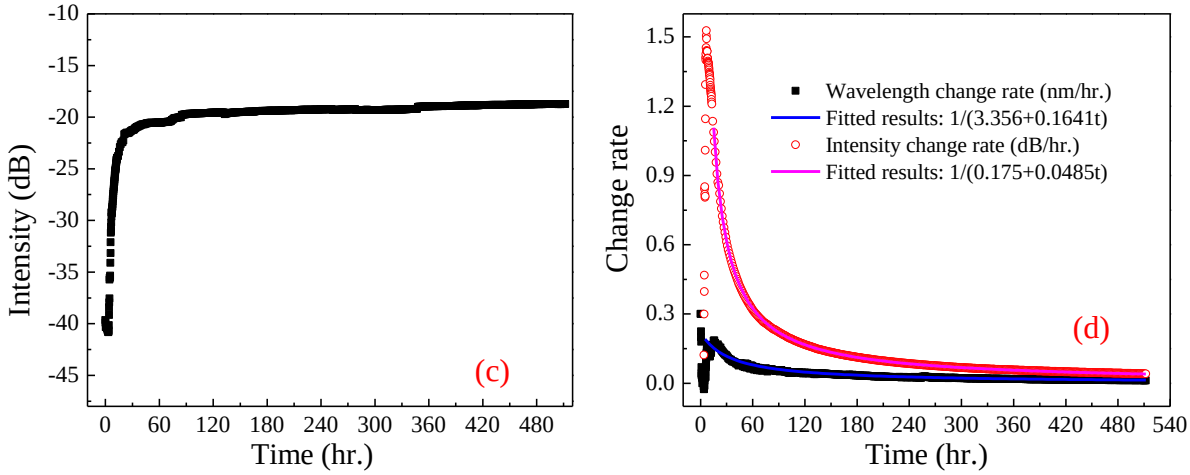

Figure 5.7 (a) Optical spectrum change of the coated LPFG through the corrosion test, (b) resonant wavelength change versus immersing time, (c) intensity change of the resonant peak versus immersing time, and (d) change rate of the resonant wavelength and its corresponding peak intensity versus immersing time

5.3.3 Discussion of Steel Corrosion Monitoring Results from Coated LPFG Sensors

From figure 5.7(b), it is known that the detection limit for the designed coating thickness was about 200 hours when using a sensor with a coating thickness of 2.5 μm. Figures 5.8(a) and (b) analyzed the observed corrosion rate related parameters of the coated LPFGs by resonant wavelength and intensity changes, respectively. In general, the corrosion process detected from the coated LPFG sensors could be divided into two stages: the first stage was within 20 hours after the rebar had been placed into the 3.5% salt water, which has a high corrosion rate observed as 0.128 nm/hr and 1.1924dB/hr; the second stage was from 20 hours after the start of the test until the detection limit (200 hours), which showed a lower corrosion rate of 0.019 nm/hr and 0.01215dB/hr. In practical applications, the initial corrosion rate vanishes so quickly that it is hard to be detected and the corrosion rate detected by other commonly used detection methods usually focuses on the stabilized corrosion rate.

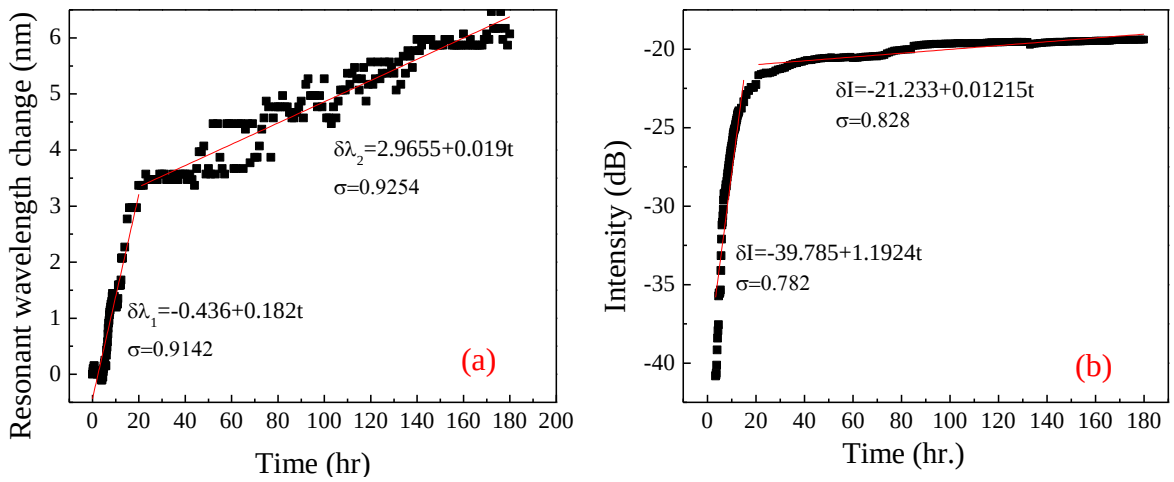

Figure 5.8 Corrosion rate obtained from the monitored results of the coated LPFG through the corrosion test: (a) Corrosion rate in resonant wavelength changes and (b) in intensity changes

5.3.4 Characterization of Coated LPFG Sensor after Corrosion Test

The characterization of the coated LPFG sensors after the accelerated corrosion test was studied using microscopic imaging tools. Figures 5.9(a) through (f) show the SEM images of the remaining coating on the fiber surface and the attached steel rust on the surface of the coating. After two months of corrosion testing, the coating on the fiber surface became very thin, as shown in figures 5.9(a) and (b) where the coating was less than 500 nm in thickness. In addition, figure 5.9(a) also shows that some coating portions on the fiber were even corroded completely. Figure 5.9(c) shows the cross section of the steel rust outside of the sensor coating. The steel rust was much thicker than the coating, with a thickness of about 20 μm. Figures 5.9(d) through (f) show the surface condition of the steel rust on the outside of the coating in different scales. The rust has a size from 500 nm to 1 μm and a porous structure.

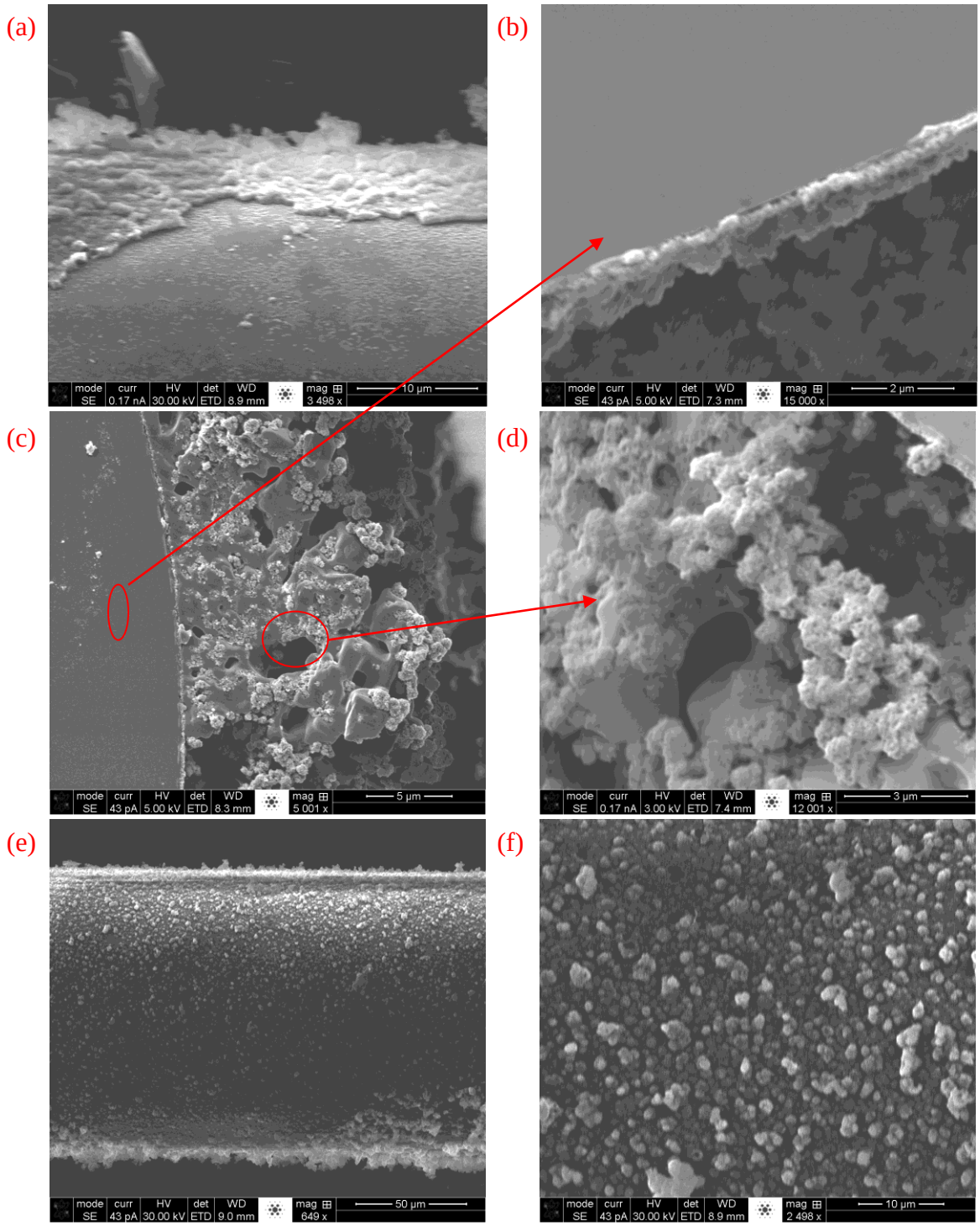

Figure 5.9 SEM images of the coated LPFG sensor after corrosion tests: (a) surface condition of the coating, (b) cross section of the remaining coating, (c) cross section of the fiber with rust on coating surface, (d) surface of the rust in large scale, (e) surface condition of the rust on the fiber surface in micro-scale, and (f) the small scale of the rust on the fiber surface

5.4 Corrosion Measurement Results from Electrochemical Studies

In addition to the proposed optical fiber sensors, electrochemical measurements were also implemented for the test steel rebar. The potentiodynamic measurements of all the test specimens were obtained by using a typical three-electrode setup, consisting of 25.4mm×25.4mm×0.254 mm platinum sheets as a counter electrode, saturated calomel electrode (SCE) as a reference electrode, and one rebar sample as a working electrode. All three electrodes were connected to a Gamry, Reference 600 potentiostat/galvanostat/ZRA for data acquisition. The corrosion resistance of the rebar samples was monitored by potentiodynamic polarization. Within the detect limit of the electrochemical method, figure 5.10 presents the corrosion rate estimated from potentiodynamic test results for all the three test samples. The average corrosion rate determined from the electrochemical method is 2.967×10^{-6}A/cm^2, with a standard deviation of 0.433×10^{-6}A/cm^2. The converted mass loss corrosion rate is then 738.783g/(m^2·day), and 34.42mm/year, with a deviation of 107.817g/(m^2·day), and 5.023mm/year.

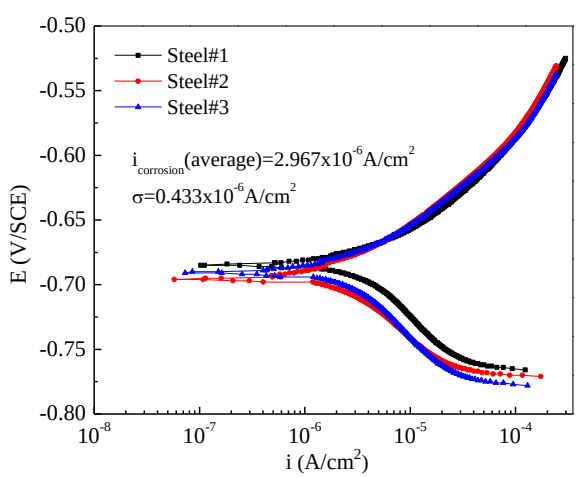

Figure 5.10 Corrosion rate estimated from potentiodynamic test results

5.5 Correlation between the Two Measurement Methods

Comparisons and correlations between the two monitoring methods were performed, with the results shown in table 5.2. The mass loss corrosion rate was calculated based on the monitoring result of the proposed LPFG sensing system. In the beginning 20 hours, the mass loss corrosion rate was found to be 4979.4g/(m^2·day). To further consider the correlation between the accelerated laboratory corrosion and the atmospheric corrosion (28-29), the atmospheric corrosion rate of the steel in the first three weeks was calculated to be 31.12g/(m^2·day) and after that was 4.65g/(m^2·day). The first few weeks seem to be especially important for prevention and mitigation of corrosion.

Table 5.2 Correlation of steel corrosion from various measurement methods

Methods	Electrochemical method (potentiodynamic test)	Mass loss (from potentiodynamic test)	Coated LPFG sensor	
			Wavelength	Intensity
Corrosion rate	2.967×10^{-6} A/cm^2	738.783 g/(m^2·day)	7.92×10-4 nm/day (0.019 nm/hr)	5×10-4dB/day (0.012dB/hr)
Converter coefficient	3.746×10^{-3} A/cm^2	9.33×105 g/(m^2·day)	1 nm/day	0.63 dB/day

5.5 Conclusions

The accelerated laboratory corrosion tests (3.5% NaCl solution immersing test) have been implemented to validate the feasibility of the proposed sensing system. The electrochemical method was also implemented for comparison and correlations. Within the detection limit of the thin coated layer, the proposed optical fiber sensors detected two different corrosion rates,

including a higher corrosion rate of 0.128 nm/hr in the beginning of 20 hours and a relative lower corrosion rate of 0.019 nm/hr afterwards. Considering that in practical applications the second stage of the corrosion rate is commonly measured by conventional measurement methods, the lower corrosion rate was used as the corrosion rate for comparison and correlation. The proposed optical fiber sensing system has a converter coefficient of 1 nm/day=3.746×10-3A/cm^2. Therefore, the proposed optical fiber sensor could monitor the critical corrosion information of the host members in real time and remotely. With multiple LPFGs in a single fiber, it is possible to provide a cost-effective corrosion monitoring technique for corrosion monitoring of large scale structures.

Chapter 6 Conclusions

In this study, a novel concept of a fiber optic corrosion sensor was demonstrated feasible for the monitoring of corrosion-induced deterioration assessment of large-scale civil transportation infrastructure. The corrosion sensor was made by coating a long period fiber grating with a thin layer of nano iron and silica particles dispersed in polyurethane. As the iron particles were gradually corroded away, the increase of resonant wavelength of the optical sensor was measured and calibrated for the purpose of corrosion monitoring. When installed near steel members and correlated with their corrosion process, a group of grating sensors could be multiplexed to monitor corrosion induced mass loss of the steel members in a bridge system or a bridge network. Based on the proof-of-concept test & steel rebar monitoring tests, the following major conclusions were drawn:

1. A thin layer of nano iron and silica particles, when dispersed in polyurethane at room temperature, was successfully coated on the surface of an LPFG to construct the corrosion sensor. To enhance the optical and mechanical properties of corrosion sensors, silica particles were added. Polyurethane was partially removed from the dried coating by heating in a furnace at 200 °C for one hour to provide a direct access of moisture to iron particles. SEM images indicated an average coating thickness of approximately 2.5 μm after heat treatment.
2. The coating process was monitored in situ to optimize the sensor fabrication procedures. The resonant wavelength of a coated grating sensor was first reduced at the dry coating state by 8.1 nm from that of the corresponding bare optical sensor, and then increased by 3.2 nm after the heat treatment, resulting in a 4.9 nm net reduction in resonant wavelength for corrosion monitoring. In comparison with an

uncoated grating sensor, the coated sensor had similar sensitivities towards the change in temperature and pH value. Therefore, the coupled temperature and pH effects on corrosion monitoring of the coated sensor could be compensated by deploying a parallel bare optical grating sensor. In comparison with the temperature effect, the pH effect on corrosion monitoring was negligible.

3. The coated corrosion sensor was tested in 3.5wt.% salt solution inside a sealed glass tube for one month. Surface and cross sectional SEM images of the coating were taken and analyzed. It was found that some iron particles were oxidized and reduced in size, causing an increase of resonant wavelength of the coated grating sensor. The thickness of the coating was reduced to approximately 2.26 μm after immersing in the 3.5% NaCl solution for one month, indicating a thickness loss of 0.24 μm or 9.6% thickness reduction compared to the initial coating thickness of 2.5 μm. On the other hand, the resonant wavelength of the coated sensor was found to rapidly increase in the first two weeks but decelerate till the end of the corrosion testing. The total increase of resonant wavelength observed at the completion of testing in one month was approximately 0.45 nm or 9% of the full extent (4.9 nm) in wavelength shift for the proposed corrosion sensor, which was in good agreement with the comparison from the SEM technique.
4. Accelerated laboratory corrosion tests (3.5% NaCl solution immersing test) were performed to validate the feasibility of the proposed sensing system. In addition to the proposed optical fiber monitoring system, the electrochemical method was also implemented for comparison and correlations. Within the detection limit of the thin coated layer, the proposed optical fiber sensors detected two different corrosion rates,

including a higher corrosion rate of 0.128 nm/hr in the beginning 20 hours and a relative lower corrosion rate of 0.019 nm/hr after. Considering that in practical applications the second stage of the corrosion rate is commonly detected by conventional measurement methods, the relative lower corrosion rate was used as the corrosion rate for comparison and correlations. The proposed optical fiber sensing system had a converter coefficient of 1nm/day or $3.746\times10\text{-}3A/cm^2$.

Future research will be directed toward correlating the corrosion process of nano iron particles with that of steel members in structural applications in various corrosive environments. The similarity and difference in the corrosion process of nano irons and steel members will be investigated as well.

References

1. Koch, G. H. 2002. "Corrosion Cost and Preventive Strategies in the United States FHWA." *FHWA-RD-01-156*, Federal Highway Administration, U.S. Department of Transportation, Washington, D.C..

2. Agarwala, V. S. and S. Ahmad. 2000. "Corrosion Detection and Monitoring – A Review: Paper No.271." *Proceedings of NACE International 2000*, Orlando, Florida.

3. ASTM. 2008. "Standard Guide for Online Monitoring of Corrosion in Plant Equipment (Electrical and Electrochemical Methods)." *Standard NO. G96-90*, ASTM International, West Conshohocken, Pennsylvania.

4. Mansfeld, F. 2003. *Electrochemical Methods of Corrosion Testing ASM Handbook.* Materials Park, Ohio: ASM International.

5. Cooper, K. R. and L. Innovations. 2001. "Optical Fiber-Based Corrosion Sensor Systems for Health Monitoring of Aging Aircraft." *Proceedings of IEEE* 128: 540-552-5.

6. Rathod, V. T., M.D. Roy, and S. Gopalakrishnan. 2006. "Lamb Wave Based Identification and Parameter Estimation of Corrosion in Metallic Plate Structure Using a Circular PWAS Array." *Proceedings of the 16th SPIE Annual Symposium on Smart Structures and Materials* 7295.

7. Steven, D. G. 2007. "Sensor Technology Innovation for the Advancement of Structural Health Monitoring: a Strategic Program of US-China Research for the Next Decade." *Smart Structures and Systems* 3: 221-244.

8. Zheng, Z., X. Sun, and Y. Lei. 2009. "Monitoring Corrosion of Reinforcement in Concrete Structures via Fiber Bragg Grating Sensors." *Frontiers of Mechanical Engineering in China* 4 (3): 316-319.

9. Hua, W., H. Cai, M. Yang, X. Tong, C. Zhou, and W. Chen. 2010. "Fe-C-coated fibre Bragg grating sensor for steel corrosion monitoring." *Corrosion Science* 53: 1933-1938.

10. Qiao, G., Z. Zhou, and J. Ou. 2006. 'Thin Fe-C Alloy Solid Film Based Fiber Optic Corrosion Sensor." *Proceedings of the 1st IEEE Conference on Nano/Micro Engineered and Molecular Systems* 541-544.

11. Christopher, K. L., T. W. Kai, and L. Chen. 2008. "A Novel Optical Fiber Sensor for Steel Corrosion in Concrete Structures." *Sensors* 8: 1960-1976.

12. Wade, S. A., C. D. Wallbrink, G. McAdam, S. Galea, B. R. W. Hinton, and R. Jones. 2008. "A Fiber Optic Corrosion Fuse Sensor Using Stressed Metal-coated Optical Fibers." *Sensors and Actuators B: Chemical* 131: 602-608.

13. Qiao, G., and J. Ou. 2007. “Corrosion Monitoring of Reinforcing Steel in Cement Mortar by EIS and ENA.” *Electrochemical Acta* 52: 8008-8019.

14. Dickerson, N. P., and S. L. Wood. 2005. “Wireless Low-cost Corrosion Sensors for Reinforced Concrete Structure.” *Proceedings of the 12th SPIE Annual Symposium on Smart Structures and Materials* 5765: 493-503.

15. Abderrahnmane, S., A. Himour, R. Kherrat, E. Chailleux, N. Jaffrezic-Renault, and G. Stremsdoerfer. 2001. “An Optical Fiber Corrosion Sensor with an Electroless Deposit of Ni–P.” *Sensors and Actuators B: Chemical* 75: 1-4.

16. Benounis, M. and N. Jaffrezic-Renault. 2004. “Elaboration of an Optical Fiber Corrosion Sensor for Aircraft Applications.” *Sensors and Actuators B: Chemical* 100: 1-8.

17. Dong, S., G. Peng, and Y. Luo. 2007. “Preparation Techniques of Metal Clad Fibers for Corrosion Monitoring of Steel Materials.” *Smart Materials and Structures* 16: 733-738.

18. Zhang, J., X. Tang, J. Dong, T. Wei, and H. Xiao. 2008. “Zeolite thin film-coated long period fiber grating sensor for measuring trace chemical.” *Optics Express* 16: 8317-8323.

19. Kim, B. H., Y. Park, T. J. Ahn, D. Y. Kim, B. H. Lee, Y. Chung, U. C. Paek, and W. T. Han. 2001. “Residual stress relaxation in core of optical fibers by CO_2 laser irradiations.” *Optics Letters* 26: 1657-1659.

20. Li, Y. J., T. Wei, J. A. Montoya, S. V. Saini, X. W. Lan, X. L. Tang, J. H. Dong, and H. Xiao. 2008. “Measurement of CO_2-laser-irradiation-induced refractive index modulation in single-mode fiber toward long- period fiber grating design and fabrication.” *Applied Optics* 47 (29): 5296-5304.

21. Bhatia, V., and A. Vengsarkar. 1996. “Optical Fiber Long Period Grating Sensor.” *Optics Letters* 21: 692-694.

22. Ivanov, O. V., S. A. Nikitov, and Y. V. Gulyaev. 2006. “Cladding modes of optical fibers: properties and applications.” *Physics Uspekhi* 49 (2): 167- 191.

23. Shu, X. W., L. Zhang, and I. Bennion. 2002. “Sensitivity Characteristics of Long-period Fiber Gratings.” *Journal of Light-wave Technology* 20(2): 255-266.

24. Shu, X. W., L. Zhang, and I. Bennion. 2001. “Fabrication and characteristics of ultra-long-period fiber gratings.” *Optics Communication* 203: 277-281.

25. Anemogiannis, E., E. N. Glytsis, and T. K. Gaylord. 2003. “Transmission characteristics of long-period fiber gratings having arbitrary azimuthal/radial refractive index variations.” *Journal of Light-wave Technology* 21 (1): 218-227.

26. Huang, Y., Z. Zhou, Y. Zhang, G. Chen, and H. Xiao. 2010. "A temperature self-compensated LPFG sensor for large strain measurements at high temperature." *IEEE Transactions on Instrumentation & Measurement* 59 (11): 2997-3004.

27. Montemor, M. F., A. M. P. Simões, and M. G. S. Ferreira. 2003. "Chloride-induced corrosion on reinforcing steel: from the fundamentals to the monitoring techniques." *Cement and Concrete Composites* 25: 491-502.

28. Drazic, D. M. and V. Vascic. 1989. "The Correlation between Accelerated Laboratory Corrosion Tests and Atmospheric Corrosion Station Tests on Steels." *Corrosion Science* 29 (10): 1197-1204.

29. Lin, C. C. and C. X. Wang. 2005. "Correlation between Accelerated Corrosion Test and Atmospheric Corrosion Tests on Steel." *Journal of Applied Electrochemistry* 35: 837-843.